

# Evolution of the Global Coupled Climate Response to Arctic Sea Ice Loss during 1990–2090 and Its Contribution to Climate Change

LANTAO SUN

*Cooperative Institute for Research in Environmental Sciences, University of Colorado Boulder, and  
Physical Sciences Division, NOAA/Earth System Research Laboratory, Boulder, Colorado*

MICHAEL ALEXANDER

*Physical Sciences Division, NOAA/Earth System Research Laboratory, Boulder, Colorado*

CLARA DESER

*Climate and Global Dynamics, National Center for Atmospheric Research, Boulder, Colorado*

(Manuscript received 5 March 2018, in final form 22 June 2018)

## ABSTRACT

The role of transient Arctic sea ice loss in the projected greenhouse gas–induced late-twentieth- to late-twenty-first-century climate change is investigated using the Geophysical Fluid Dynamics Laboratory’s Coupled Model version 3. Two sets of simulations have been conducted, one with representative concentration pathway (RCP) 8.5 radiative forcing and the second with RCP forcing but with Arctic sea ice nudged to its 1990 state. The difference between the two five-member sets indicates the influence of decreasing Arctic sea ice on the climate system. Within the Arctic, sea ice loss is found to be a primary driver of the surface temperature and precipitation changes. Arctic sea ice depletion also plays a dominant role in projected Atlantic meridional overturning circulation weakening and changes in North Atlantic extratropical sea surface temperature and salinity, especially in the first half century. The effect of present-day Arctic sea ice loss on Northern Hemisphere (NH) extratropical atmospheric circulation is small relative to internal variability and the future sea ice loss effect on atmospheric circulation is distinct from the projected anthropogenic change. Arctic sea ice loss warms NH extratropical continents and is an important contributor to global warming not only over high latitudes but also in the eastern United States. Last, the Arctic sea ice loss displaces the Pacific intertropical convergence zone (ITCZ) equatorward and induces a “mini-global warming” in the tropical upper troposphere.

## 1. Introduction

Arctic sea ice extent has declined rapidly over the past three decades, likely resulting from increased poleward heat transport and local radiative feedbacks associated with an increase in greenhouse gases (e.g., Park et al. 2015). Internal climate variability may also have contributed to sea ice loss (e.g., Mahajan et al. 2011; Day et al. 2012; Yeager et al. 2015; Zhang 2015; Ding et al. 2017; Lee et al. 2017; Li et al. 2017, 2018). Climate

models forced by increasing greenhouse gas (GHG) concentrations project an ice-free Arctic Ocean during summer by the mid-to-late twenty-first century (e.g., Stroeve et al. 2012; Wang and Overland 2012). The disappearing sea ice can affect the atmosphere and ocean locally and remotely. Within the Arctic, near-surface air temperature rises much faster than in the lower latitudes (Screen and Simmonds 2010). Arctic precipitation also increases (Deser et al. 2010), dominated by rain near the end of the twenty-first century, especially in the warm seasons (Bintanja and Andry 2017). With full ocean–atmosphere coupling, the signals associated with Arctic sea ice change can be seen in the tropics, and even as far as Antarctica (e.g., Deser et al. 2015).

The remote effect of Arctic sea ice reduction on Northern Hemisphere (NH) midlatitude weather and

---

Supplemental information related to this paper is available at the Journals Online website: <https://doi.org/10.1175/JCLI-D-18-0134.s1>.

---

Corresponding author: Dr. Lantao Sun, [lantao.sun@noaa.gov](mailto:lantao.sun@noaa.gov)

climate has been investigated for several decades. By prescribing Arctic sea ice concentration changes in atmospheric general circulation models (AGCMs), many previous studies have addressed the extent to which Arctic sea ice loss influences the large-scale atmospheric circulation and surface climate. For example, [Deser et al. \(2004\)](#) found that sea ice loss–induced circulation changes are composed of a local baroclinic structure with the surface trough and upper-level ridge and an equivalent barotropic structure that resembles the negative phase of the North Atlantic Oscillation (NAO)/northern annular mode (NAM). Also, several AGCM experiments have suggested that most of the midlatitude continents warm in response to a reduction in sea ice with the exception of central/eastern Asia, where weak cooling may appear in relation to an enhanced Siberian high (e.g., [Peings and Magnusdottir 2014](#); [Screen et al. 2015a](#); [Sun et al. 2015](#); [Semmler et al. 2016](#)). These studies, however, cannot be used to address the questions associated with the ocean change and ocean–atmosphere coupling because the lower boundary conditions are specified.

More recently, some studies have utilized coupled atmosphere–ocean general circulation models (AOGCMs) to investigate the global climate response to Arctic sea ice loss, either by altering the sea ice parameters such as albedo (e.g., [Bitz et al. 2006](#); [Winton 2008](#); [Scinocca et al. 2009](#); [Graversen and Wang 2009](#); [Blackport and Kushner 2016, 2017](#); [Cvijanovic et al. 2017](#)) or by adding an additional heat flux to the sea ice throughout the simulation (“ghost forcing”; [Deser et al. 2015](#); [Deser et al. 2016](#); [Tomas et al. 2016](#); [Oudar et al. 2017](#)) or by sea ice nudging ([McCusker et al. 2017](#); [Smith et al. 2017](#)). Arctic sea ice loss imposes surface heat and freshwater into the ocean, and thus has the potential to influence ocean circulation, including the density-driven Atlantic meridional overturning circulation (AMOC), whose northern boundary interacts with Arctic sea ice (e.g., [Li et al. 2017](#)). The AMOC weakens in response to an abrupt reduction in sea ice ([Bitz et al. 2006](#); [Winton 2008](#); [Scinocca et al. 2009](#); [Blackport and Kushner 2016](#); [Tomas et al. 2016](#); [Oudar et al. 2017](#)), in agreement with the projected decline in simulations from phase 5 of the Coupled Model Intercomparison Project (CMIP5) ([Cheng et al. 2013](#); [Collins et al. 2013](#)). In addition, [Sévellec et al. \(2017\)](#) examined the sensitivity of the AMOC to the surface heat and freshwater fluxes and suggested that 75% of the observed AMOC decline is driven by Arctic sea ice changes. In these aforementioned sea ice experiments, the “North Atlantic warming hole,” with little warming or even a decrease in sea surface temperatures (SSTs) to the south of Greenland, appears to be associated with the slowing of

the AMOC ([Cheng et al. 2013](#); [Collins et al. 2013](#); [Tomas et al. 2016](#)).

With ocean–atmosphere coupling, Arctic sea ice loss can impact the tropical ocean and the location of the intertropical convergence zone (ITCZ), but the response varies depending on the type of ocean coupling. [Deser et al. \(2015\)](#) conducted experiments with the Community Climate System Model version 4 (CCSM4), which includes an ocean general circulation model (GCM). They found that the projected Arctic sea ice loss caused the ITCZ to be displaced toward the equator. Moreover, as a result of enhanced equatorial convection and latent heat release, zonal-mean temperature increases in the tropical upper troposphere, resembling a “mini-global warming” due to increased GHG emissions. With ocean dynamics disabled by using a slab-ocean model in place of the ocean GCM, the ITCZ is displaced northward, toward the hemisphere in which sea ice declines ([Deser et al. 2015](#); [Tomas et al. 2016](#)), which is consistent with similar studies that use slab-ocean coupled models (e.g., [Chiang and Bitz 2005](#); [Broccoli et al. 2006](#); [Frierson and Hwang 2012](#); [Cvijanovic et al. 2017](#)) or fully coupled models that constrained ocean temperature and salinity below 200 m ([Smith et al. 2017](#)). The sensitivity of the ITCZ response to ocean coupling is closely connected to the cross-equatorial northward heat transport accomplished by both the ocean and atmosphere ([Deser et al. 2015](#); [Tomas et al. 2016](#); [Kay et al. 2016](#)). In the NH extratropics, the ocean–atmosphere coupling can magnify the atmospheric response to Arctic sea ice loss as compared to atmosphere-only simulations but does not change its overall structure, given that both dynamical and thermodynamical processes have been included for a proper representation of oceanic feedbacks ([Deser et al. 2016](#)).

Most previous studies have focused on the equilibrium climate response to an abrupt Arctic sea ice loss and only few looked at the transient evolutions. For example, [Blackport and Kushner \(2016\)](#) compared the extratropical response in equilibrium with that averaged over the first 50 years. [Wang et al. \(2018\)](#) explored the tropical response using full ocean coupled and slab-ocean coupled AOGCMs and found that ocean dynamics become important within two decades of a sudden loss of sea ice, considerably faster than often assumed ([Cvijanovic et al. 2017](#)). Moreover, in these experiments the sea ice depletion occurs abruptly at the beginning, and thus the transient response to sea ice loss cannot be directly compared with the transient change in fully forced climate projections, whose ice forcing increases with time. And abrupt sea ice loss studies cannot be used to tell how much the present-day sea ice reduction may affect the NH jet stream either, a topic still in debate [see two distinct perspectives in [Barnes](#)

and Screen (2015) and Francis et al. (2017); see also references therein].

The goal of this study is to comprehensively evaluate the contributions of transient Arctic sea ice loss to the projected global climate change over the twenty-first century in a fully coupled climate model. While previous studies investigated the equilibrium response to an abrupt sea ice decline, we focus on the transient response to a gradually increasing projected Arctic sea ice loss, which bridges the gap between present-day and future sea ice conditions and their potential impact on the climate system. The rest of this paper is organized into four sections. Section 2 contains a description of the model used here, the Coupled Model version 3 (CM3) from the Geophysical Fluid Dynamics Laboratory (GFDL), and the experimental design. Section 3 presents the effects of transient Arctic sea ice loss on the ocean and atmosphere and their contributions to the total anthropogenic global climate change, including the responses in the Arctic, NH extratropics, and tropics. Discussion and conclusions follow in section 4.

## 2. Model and experimental design

### a. Model description

CM3 (version Ulm\_201505) is composed of version 3 of the atmospheric model (AM3), the Modular Ocean Model version 5 (MOM5), a sea ice model, and land model components. AM3 uses a cubed-sphere implementation of a finite-volume dynamical core with the horizontal resolution of approximately 200 km (Donner et al. 2011). The vertical resolution ranges approximately from 70 m near Earth's surface to 1–1.5 km near the tropopause and 3–4 km in much of the stratosphere, with the top model level at approximately 80 km (Donner et al. 2011). Compared to the previous version of the atmosphere model (AM2), AM3 includes a more comprehensive treatment of the indirect effect of aerosols and cloud drop number concentrations (Golaz et al. 2011). The horizontal resolution of MOM5 is 1° in latitude with enhanced meridional resolution equatorward of 30°N/S that reaches 1/3° at the equator (Griffies et al. 2011). The sea ice model, documented in Delworth et al. (2006) and Winton (2000), uses the same horizontal grid arrangement as the ocean model. The Arctic sea ice concentration and thickness in CM3 are in better agreement with observations than in the previous version of the model (CM2; Griffies et al. 2011; Li et al. 2018).

### b. Experimental design

We conducted two types of transient simulations. First, a five-member ensemble of CM3 simulations were performed over the period 1970–2090 by following the

CMIP5 historical and representative concentration pathway 8.5 (RCP8.5) protocol (denoted as RCP hereafter) to characterize the “full” global climate change. This is a business-as-usual scenario in which the radiative forcing will reach  $8.5 \text{ W m}^{-2}$  by 2100 (Riahi et al. 2011). This simulation allows us to calculate the climate response to total anthropogenic forcing by calculating the difference from 1971–90 climatology:

$$\Delta\text{RCP}(\text{year}) = \text{RCP}(\text{year}) - \text{RCP}(1971 - 90), \quad (1)$$

where “year” varies from 1990 to 2090. To isolate the Arctic sea ice loss effect, five corresponding RCP simulations were conducted with the Arctic sea ice volume artificially relaxed to a repeating seasonal cycle of 1990 sea ice conditions in each ensemble member (denoted as RCP\_ICE1990 hereafter). The initial condition of each member of RCP\_ICE1990 also comes from 1 January 1990 of the corresponding RCP simulation to avoid any discontinuity. This simulation can tell the climate response to anthropogenic forcing without Arctic sea ice changes, which is

$$\begin{aligned} \Delta\text{RCP\_ICE1990}(\text{year}) \\ = \text{RCP\_ICE1990}(\text{year}) - \text{RCP}(1971 - 90). \end{aligned} \quad (2)$$

The difference between  $\Delta\text{RCP}$  and  $\Delta\text{RCP\_ICE1990}$  can be solely attributed to the effect of projected transient Arctic sea ice loss, referred to as

$$\begin{aligned} \Delta\text{ICE}(\text{year}) = \Delta\text{RCP}(\text{year}) - \Delta\text{RCP\_ICE1990}(\text{year}) \\ = \text{RCP}(\text{year}) - \text{RCP\_ICE1990}(\text{year}), \end{aligned} \quad (3)$$

where the same climatological reference is used to define the temporal difference in both experiments, so  $\Delta\text{ICE}$  reduces to the difference between experiments for the time period being examined. Note that in our experiments,  $\Delta\text{ICE}$ , the sea ice loss effect, is derived indirectly, different from some previous studies that keep radiative forcing fixed with a change in sea ice being the only forcing (e.g., Deser et al. 2015; Blackport and Kushner 2016; Wang et al. 2018). However, it has been shown that the effect of sea ice loss in the overall change to increasing GHG is quite linear (McCusker et al. 2017), suggesting that our results may still be compared with those studies. While choosing the 1990 start time insures the simulations are identical at their start, there is a small mismatch between the climate change effect (relative to 1971–90 climatology) and sea ice loss effect (relative to 1990 conditions) such that the fraction of sea ice loss contribution ( $\Delta\text{ICE}/\Delta\text{RCP}$ ) may be slightly underestimated, especially in the initial years. The statistical significance is evaluated using two-sided

Student's  $t$  test based on the ensemble mean by treating each year to be an independent sample.

The sea ice volume nudging technique (Knutson 2003) in RCP\_ICE1990 is very similar to the method described in McCusker et al. (2017) and works continuously to the ice model over the course of the simulations. At each time step, the model calculates the enthalpy needed to convert the Arctic sea ice volume to the target (i.e., the RCP 1990 value). This enthalpy is then applied to the bottom of the ice via a time-varying “ghost flux”:

$$\mathbf{Q}_{\text{flux}} = \frac{L_{\text{ice}} D_{\text{ice}} (C_{\text{ice}} h_{\text{ice}} - C_{\text{ice}_t} h_{\text{ice}_t}) dt}{\tau_{\text{ice}}}, \quad (4)$$

where  $L_{\text{ice}}$  is the latent heat of fusion ( $3.34 \times 10^5 \text{ J kg}^{-1}$ ),  $D_{\text{ice}}$  is the density of ice ( $905 \text{ kg m}^{-3}$ ),  $C_{\text{ice}}$  is the sea ice concentration (%),  $h_{\text{ice}}$  is the sea ice thickness (m),  $C_{\text{ice}_t}$  is the target sea ice concentration,  $h_{\text{ice}_t}$  is the target sea ice thickness,  $dt$  is the time step (2 h), and  $\tau_{\text{ice}}$  is the relaxation time (5 days). We also account for the changes in snow layer above the ice when calculating the  $\mathbf{Q}_{\text{flux}}$ . When conducting the nudging, the  $\mathbf{Q}_{\text{flux}}$  is only applied to the sea ice model and does not directly interact with the ocean. Moreover, the ice bottom temperature is fixed at freezing in the model (Winton 2000), so the nudging does not artificially cool the underlying Arctic Ocean (not shown). The nudging itself does not appear to impact the AMOC, either. In the RCP simulation when the sea ice is nudged to that in the RCP, the AMOC response also tends to follow that in RCP and diverges from that in RCP\_ICE1990 (not shown). While energy is not conserved in the nudged RCP\_ICE1990 simulations, effort has been made to conserve the water flux across the atmosphere–ice–ocean interface so that the global water mass budget is always conserved. Additionally, there are some grid points around Greenland with unrealistically high ice thickness (more than 40 m, up to  $\sim 600$  m) in the RCP simulations. Conducting nudging in these grid points caused the model to crash. To resolve that issue, smaller values have been used in both initial condition and the ice volume target in RCP\_ICE1990. Since sea ice volume is always nudged to the 1990 condition, this did not affect the surface heat and freshwater budgets.

### 3. Results

#### a. Arctic sea ice loss and surface energy flux response

Figure 1 shows the March and September Arctic sea ice concentrations during 1971–90, 2011–50, 2051–90, and the Arctic sea ice extent (SIE) evolution in RCP simulations (black curves). The climatological sea ice concentration and SIEs in March and September are both in good agreement with observations (observed

concentration not shown; green curves indicate observed SIEs from National Snow and Ice Data Center) (Fetterer et al. 2017). With increasing GHG concentrations, Arctic sea ice declines rapidly and the simulated SIE trend is slightly larger than in observations during 1979–2017. The Arctic Ocean becomes ice-free (defined as the year of sea ice extent minimum less than 1 million  $\text{km}^2$ ) in the ensemble mean during summer by 2026 ( $\sim 2040$  if based on August SIE), a few decades earlier than the ensemble mean of the models from CMIP5 and the Community Earth System Model (CESM) Large Ensemble (Wang and Overland 2012; Jahn et al. 2016). The faster sea ice decline in CM3 RCP simulations might be partly related to the stronger atmospheric response to the reduction of future anthropogenic aerosol emissions through the indirect effects of aerosols, increasing the climate sensitivity (Andrews et al. 2012). The Arctic sea ice extent in RCP\_ICE1990 is also shown in Figs. 1b and 1c (red curves). As a result of sea ice nudging, Arctic sea ice extent, concentration, and thickness remain close to the corresponding RCP 1990 conditions even though the radiative forcing increases following the RCP8.5 protocol (Figs. 1b,c; see also Fig. S1 in the online supplemental material).

Sea ice loss impacts the atmosphere and ocean locally via surface energy fluxes (i.e., the latent heat flux, sensible heat flux, longwave radiative flux, and net solar radiative flux). (Note that ocean can be heated by solar radiation but the atmosphere is effectively transparent to it.) The monthly change of SIE between 1971–90 and 2051–90 (bars) and the Arctic surface energy flux response in  $\Delta\text{ICE}$  (curves; obtained by differencing the RCP and RCP\_ICE1990 averaged over climatological March SIE region and over 2051–90) are shown in Fig. 2. During 2051–90, the maximum sea ice loss appears in June–July and November–December; in contrast, the maximum loss occurs in September–October during 2011–50 (Fig. S2). In agreement with previous studies (e.g., Deser et al. 2010), Arctic sea ice loss induces more upward heat flux into the atmosphere especially in winter (Fig. 2a). Sea ice loss warms the Arctic Ocean mostly in summer through downward solar radiation as a result of surface albedo decrease and disappearing ice barrier, which is partly offset by the upward heat flux across the ocean–ice–atmosphere surface (Fig. 2b). In winter, because of the lack of solar radiation, sea ice loss is only responsible for strong fluxes from the ocean to the atmosphere (bottom right panels of Figs. 2a and 2b). The upward surface heat fluxes in the sea ice loss regions are accompanied by downward fluxes farther south. This dipole pattern is a common feature in AGCM and AOGCM sea ice experiments (e.g., Deser et al. 2010; Sun et al. 2015; Oudar et al. 2017) and can be explained as

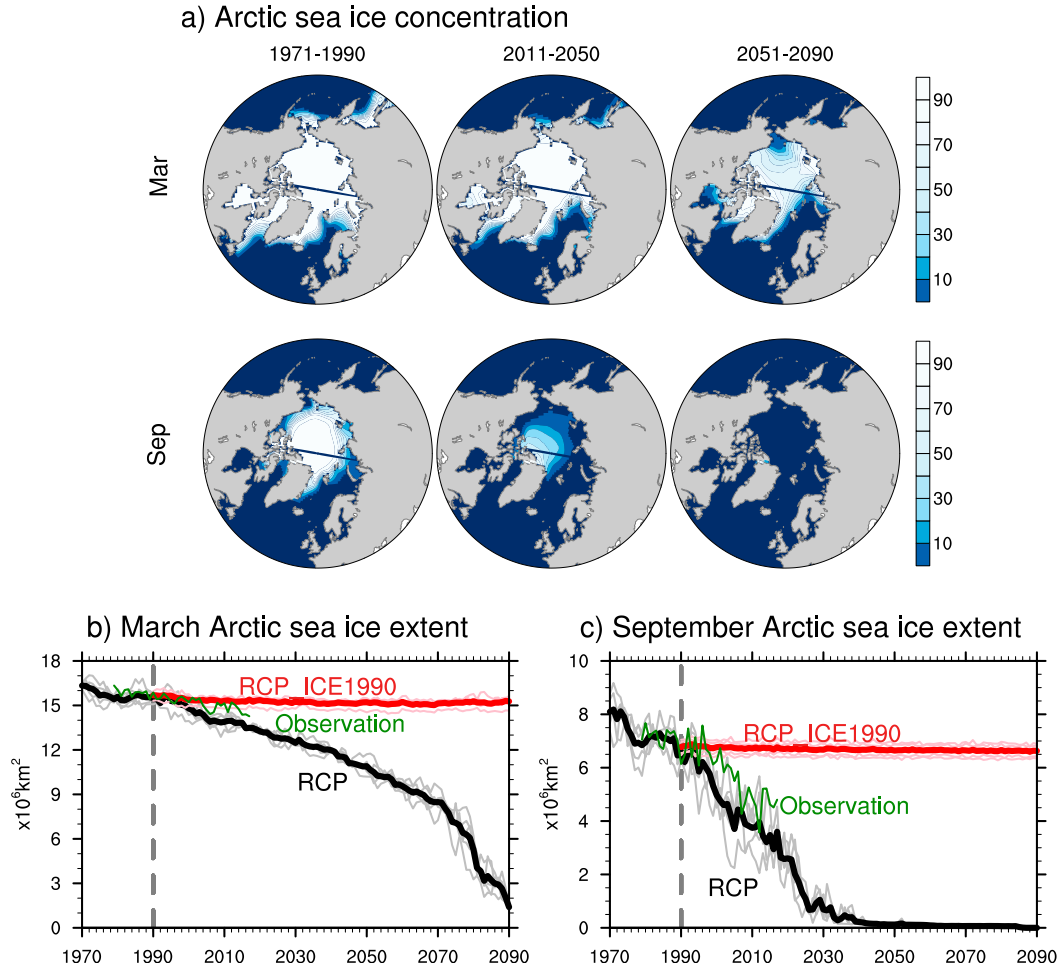


FIG. 1. (a) Arctic sea ice concentration (%) averaged over (left) 1971–90, (middle) 2011–50, and (right) 2051–90 in RCP experiments. (b) March Arctic sea ice extent ( $10^6 \text{ km}^2$ ) from CM3 RCP and RCP\_ICE1990 experiments. (c) As in (b), but for sea ice extent in September. Thin gray (pink) curves denote the RCP (RCP\_ICE1990) individual members and thick curve denotes the ensemble mean. Green curves show the observed values from National Snow and Ice Data Center. Blue lines in (a) are due to polar projections on tripolar grids.

advection of anomalous warm air due to sea ice loss to the surrounding region imposing downward heat fluxes. In the North Atlantic, part of the downward heat flux is related to the SST cooling as a result of ocean circulation changes, as will be discussed in the next subsection. All these features are robust for both 2011–50 and 2051–90, with greater magnitudes in the later period (Fig. 2 and Fig. S2).

*b. Arctic climate change*

Figures 3a and 3b show the seasonal cycles of Arctic near-surface air temperature and SST responses in  $\Delta\text{ICE}$  (RCP minus RCP\_ICE1990; blue bars) and  $\Delta\text{RCP}$  [RCP minus RCP(1971–90); black bars] averaged over 2011–50 (filled bars) and 2051–90 (empty bars), while the sea ice contribution to the total change ( $\Delta\text{ICE}/\Delta\text{RCP}$ ) is shown in Fig. 3d. Here, “Arctic” is defined as the region encompassing the climatological March SIE;

similar results are obtained using the climatological monthly SIE (not shown). Consistent with the surface energy flux response, the maximum atmospheric warming occurs in winter while the maximum oceanic SST warming occurs in summer in  $\Delta\text{ICE}$ , with larger magnitudes over 2051–90 compared to 2011–50. About 60%–80% of the projected SST warming in  $\Delta\text{RCP}$  occurs in  $\Delta\text{ICE}$  over 2011–50 and the sea ice loss contribution increases to 80%–90% over 2051–90, indicating that the future Arctic Ocean SST change is primarily due to sea ice loss. The contribution of sea ice loss to the projected near-surface air temperature response is similar between two periods and seasonally dependent, with the largest contribution (~80%) in winter and smallest contribution (~40%–50%) in summer.

Figures 3c and 3d show the 2011–50 and 2051–90 averaged precipitation responses in  $\Delta\text{ICE}$ ,  $\Delta\text{RCP}$ , and

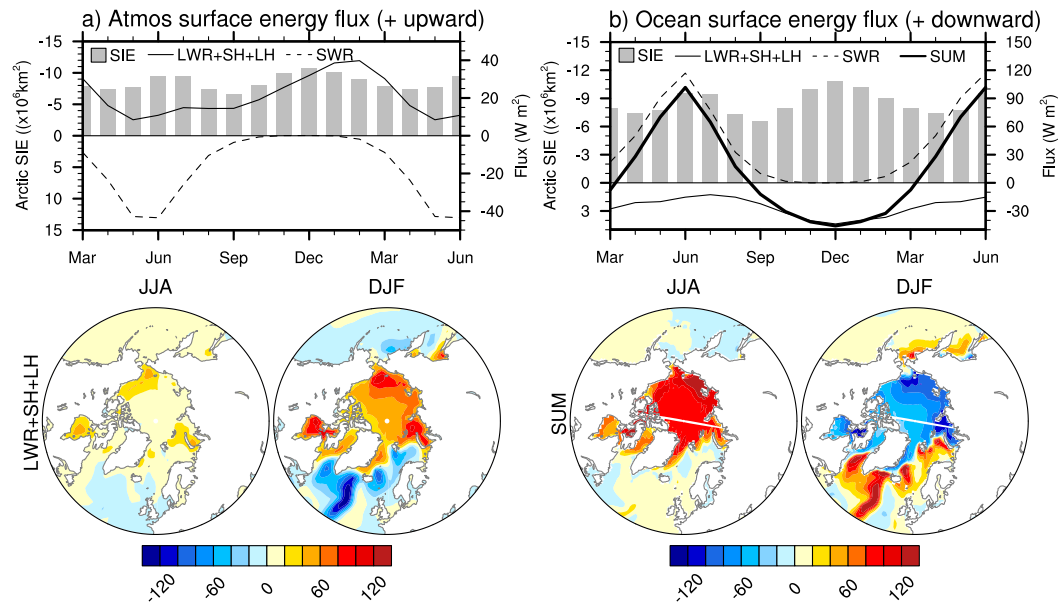


FIG. 2. (a) (top) Monthly change of SIE between 1971–90 and 2051–90 (gray bars;  $10^6 \text{ km}^2$ ), and Arctic atmospheric surface energy flux ( $\text{W m}^{-2}$ ; positive upward) response in  $\Delta \text{ICE}$  (obtained by differencing the RCP and RCP\_ICE1990 and averaged over the climatological March SIE region) during 2051–90. Atmospheric surface energy flux includes longwave radiative flux (LWR), sensible heat (SH), and latent heat (LH) flux. Shortwave radiative flux (SWR) is displayed separately. (bottom) Atmospheric surface energy flux response in (left) JJA and (right) DJF. (b) As in (a) but for the ocean surface energy flux response (positive downward). Ocean surface energy flux includes SWR, LWR, SH, and LH. Contour interval is  $20 \text{ W m}^{-2}$ . Note that (a) is obtained from atmosphere model output and (b) is obtained from ocean model output. White lines in the bottom panel of (b) are due to polar projections on tripolar grids.

$\Delta \text{ICE}/\Delta \text{RCP}$ , indicating an even larger seasonal dependence than the temperature response. In particular, sea ice loss induces  $\sim 0.2 \text{ mm day}^{-1}$  precipitation increases in winter over 2011–50, accounting for about 80% of projected precipitation change. In summer, by contrast, Arctic precipitation increases by less than  $0.05 \text{ mm day}^{-1}$  in response to disappearing sea ice, accounting for only  $\sim 10\%$ – $20\%$  of the projected change. A similar fraction of the sea ice loss contribution also appears in 2051–90, although the magnitudes in both  $\Delta \text{ICE}$  and  $\Delta \text{RCP}$  are larger. As a result of atmospheric warming, the Arctic precipitation increase in the late twenty-first century is dominated by rain instead of snow, especially in April–November (Fig. S3; Bintanja and Andry 2017). The contribution from sea ice loss to the projected changes in rain and snow are similar to the total precipitation, ranging from  $\sim 15\%$  in summer to  $\sim 80\%$  in winter.

One may wonder how different the Arctic climate response will be once sea ice is completely gone in September. Figure S4 shows the September near-surface air temperature and SST response time series in  $\Delta \text{ICE}$  and  $\Delta \text{RCP}$ . The Arctic temperature appears to continue warming in  $\Delta \text{ICE}$  after the ice-free period ( $\sim 2026$ ). One possible explanation is that sea ice loss in other seasons may still contribute a continuation of the warming in the

atmosphere and ocean in September. This is further explored by checking the evolution of September Arctic surface energy flux response to sea ice loss (Fig. S5). While the shortwave flux response appears to be nearly stable after the ice-free period, the longwave flux and latent heat flux responses continue to increase. This suggests that sea ice loss effect continues to increase in September even after September is ice-free.

### c. North Atlantic Ocean response

The AMOC response time series in  $\Delta \text{ICE}$  and  $\Delta \text{RCP}$  are shown in Figs. 4a and 4d. Following previous studies (e.g., Cheng et al. 2013; Oudar et al. 2017) an AMOC index is defined as the annual-mean maximum volume transport streamfunction at  $30^\circ \text{N}$ , although the index trend was not sensitive to the selected latitude. For model ensemble mean, AMOC declines by  $\sim 6 \text{ Sv}$  ( $1 \text{ Sv} \equiv 10^6 \text{ m}^3 \text{ s}^{-1}$ ) during 1990–2090 in response to Arctic sea ice reduction and roughly two-thirds occur in the first 20 years (estimated based on 20-yr running mean; shown by dashed red curve). But there is a fair bit of variability among different ensemble members and these differences in the trend may partly be caused by the natural variability. The total AMOC decline during 1990–2090 ( $\sim 6 \text{ Sv}$ ) is larger than in Tomas et al. (2016)

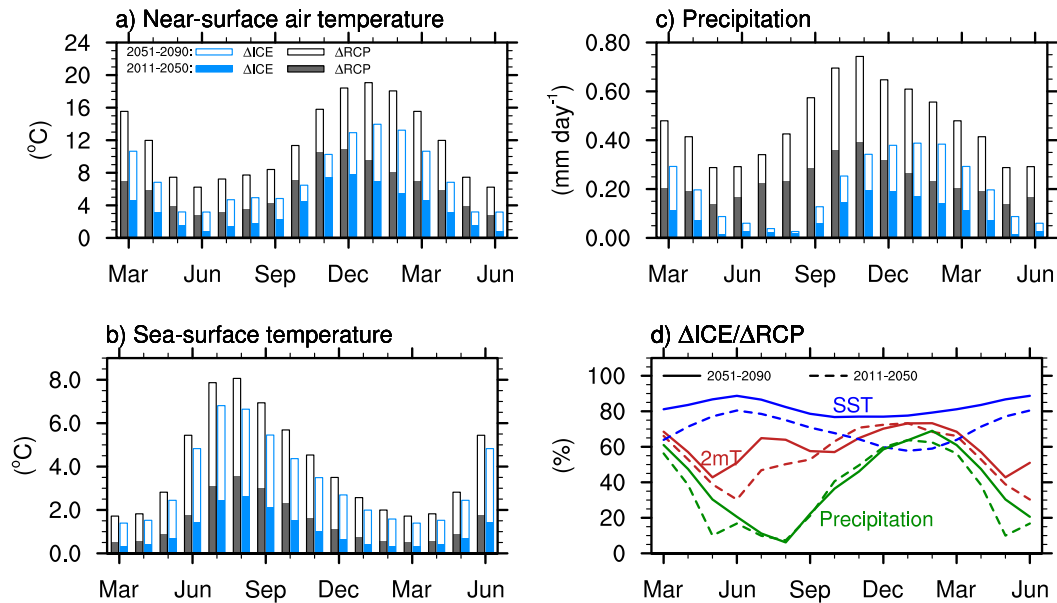


FIG. 3. (a) Monthly change of Arctic near-surface air temperature ( $^{\circ}\text{C}$ ) responses in  $\Delta\text{ICE}$  (blue bars; RCP minus RCP\_ICE1990) and  $\Delta\text{RCP}$  [black bars; RCP minus RCP(1971–90)] averaged over 2011–50 (filled bars) and 2051–90 (empty bars). (b) As in (a), but for the Arctic sea surface temperature ( $^{\circ}\text{C}$ ) responses. (c) As in (a), but for the Arctic precipitation ( $\text{mm day}^{-1}$ ) responses. (d) Seasonal cycle of the fraction (%) of  $\Delta\text{ICE}/\Delta\text{RCP}$ . In (a)–(c), the Arctic is defined as the region of climatological Arctic sea ice extent in March.

and Blackport and Kushner (2016) ( $\sim 2\text{ Sv}$ ) but close to that in Oudar et al. (2017). Moreover, the sea ice loss-induced transient AMOC change is quite different from the change in RCP simulations, which shows a quasi-linear decrease of  $\sim 1.2\text{ Sv}$  per decade and exhibits much smaller natural variability. During 1990–2090, the AMOC decreases by  $\sim 12\text{ Sv}$  in RCP simulations and roughly half of it ( $\sim 6\text{ Sv}$ ) is driven by the transient Arctic sea ice loss. Figures 4b,e and 4c,f show the AMOC streamfunction in  $\Delta\text{ICE}$  and  $\Delta\text{RCP}$  during 2011–50 and 2051–90, respectively, as a function of latitude and depth. In agreement with the time series in Figs. 4a and 4d, the sea ice loss-induced streamfunction can explain most of the projected decline during 2011–50 and this fraction becomes smaller during 2051–90 as AMOC largely stabilizes in response to projected sea ice loss but it continues to decline under anthropogenic climate change.

The ocean circulation change is accompanied by changes in SSTs. The top panels of Fig. 5 show the annual North Atlantic SST response in  $\Delta\text{ICE}$  and  $\Delta\text{RCP}$  during four 20-yr periods after 2010. In response to Arctic sea ice loss, SST increases mostly over marginal seas (e.g., Hudson Bay and areas surrounding Greenland). Weak SST warming also appears in the lower-latitude Atlantic Ocean especially in 2071–90. Near  $50^{\circ}\text{--}60^{\circ}\text{N}$ ,  $27^{\circ}\text{--}37^{\circ}\text{W}$  (box), there is a small region of SST cooling in  $\Delta\text{ICE}$ . Similar cooling also appears in  $\Delta\text{RCP}$  and other full climate change simulations (e.g.,

Collins et al. 2013) and is commonly referred to as the North Atlantic warming hole (NAWH). The NAWH has been found to be closely related to the AMOC decline [see Fig. 6 in Cheng et al. (2013)], part of which can be attributed to the Arctic sea ice depletion (e.g., Deser et al. 2016; Sévellec et al. 2017; Suo et al. 2017).

The NAWH in  $\Delta\text{ICE}$  and  $\Delta\text{RCP}$  also evolves with time (Fig. 5, top panels). During 2011–30, the SST cooling region in  $\Delta\text{ICE}$  is well beyond the box, extending farther westward and southward. Over time, the magnitude of the cold SSTs gradually weakens and shifts to the southeast corner of the region due to warming on the west side of the NAWH and such warming appears to come primarily from the sensible heat flux (not shown). The SST evolution in  $\Delta\text{RCP}$  is similar to  $\Delta\text{ICE}$ , but the NAWH simply weakens and shrinks inside the box region. The bottom panel in Fig. 5 shows the time series of the NAWH SST response in  $\Delta\text{ICE}$  and  $\Delta\text{RCP}$ . In response to transient Arctic sea ice loss, annual SST first decreases following the decline of AMOC, then transitions back to warming by late twenty-first century while AMOC weakening persists. Similar SST evolution also appears in  $\Delta\text{RCP}$ , but with smaller magnitude of cooling likely due to the compensation of surface warming by increased radiative forcing. Moreover, the NAWH SST in  $\Delta\text{ICE}$  and  $\Delta\text{RCP}$  both exhibit a well-defined seasonal change, with cooling to be stronger in winter and weaker (or even warming) in summer (Fig. 5,

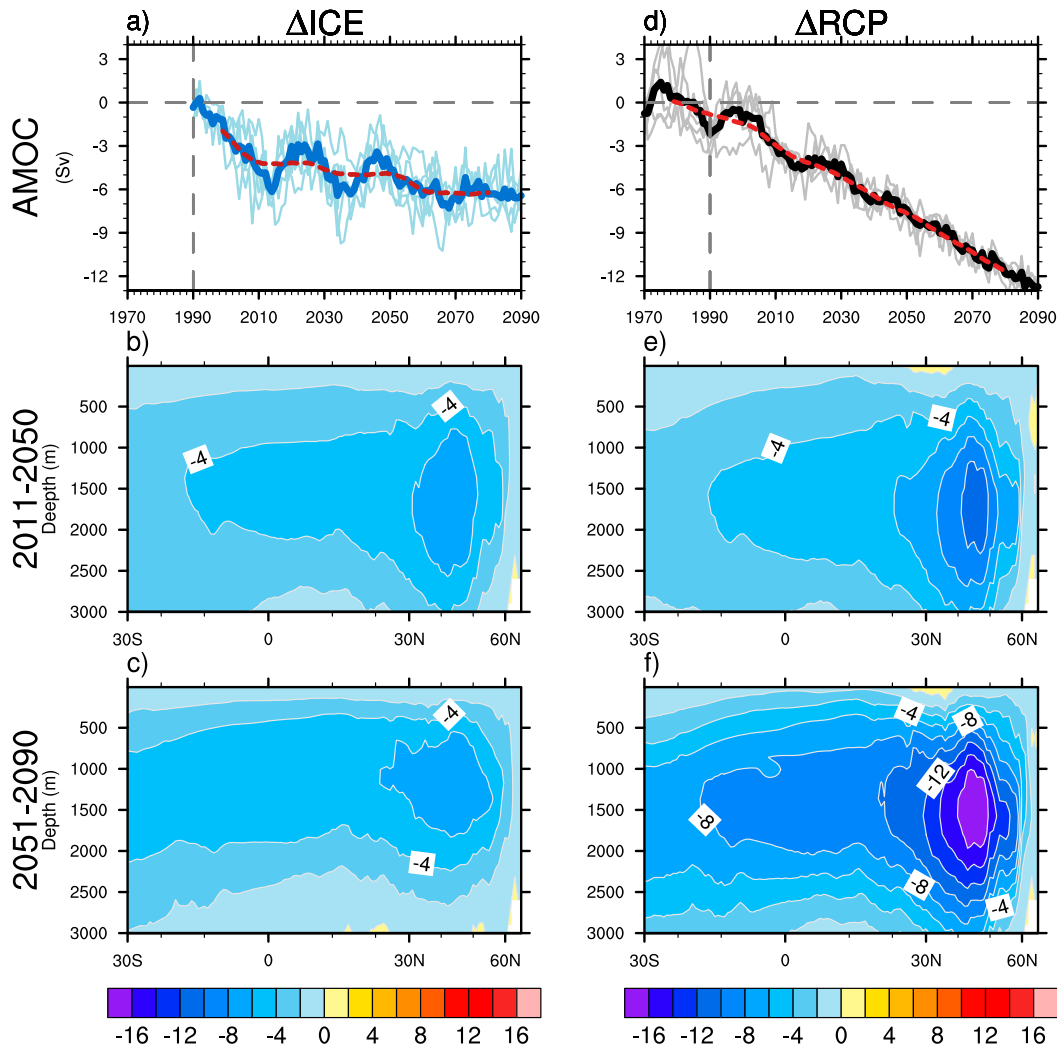


FIG. 4. (a),(d) Time series of AMOC response (in Sv) in  $\Delta$ ICE and  $\Delta$ RCP, respectively. Thin blue curves denote the individual members and thick blue curve indicate ensemble mean. Dashed red curve indicates the smoothed blue curve using 20-yr running mean. (b),(e) Latitude–depth cross section of the AMOC streamfunction averaged over 2011–50 in  $\Delta$ ICE and  $\Delta$ RCP, respectively. (c),(f) As in (b),(e), but averaged over 2051–90. Contour interval is 2 Sv.

bottom panel). This also occurs in observations of AMOC (Caesar et al. 2018). It is likely related to the seasonal cycle in the ocean mixed-layer depth, which is much shallower in summer than in winter so that the greenhouse gas–induced warming from the atmosphere is confined to a much thinner layer (Alexander et al. 2018) and AMOC has a much smaller effect on SSTs in summer.

The corresponding annual North Atlantic sea surface salinity (SSS) responses in  $\Delta$ ICE and  $\Delta$ RCP are shown in Fig. 6. In response to continued sea ice loss, the salinity shows a freshening of the surface water at North Atlantic subpolar gyre and an increase in salinity in the subtropical gyre. The freshening near the Arctic is likely related to the increased freshwater flux as a result of sea ice melting and overall increased precipitation (Fig. S6).

In addition, the SSS response may be partly related to the change in AMOC due to its similarity to the AMOC regression pattern (Cheng et al. 2013). For example, the freshening around the NAWH is largely explained by the increase in precipitation minus evaporation (Fig. S7) as a result of decrease in evaporation (not shown). There is a strong resemblance between sea ice loss–induced salinity change and the projected RCP change. Arctic sea ice loss can explain the majority of the salinity decrease in the mid-to-high latitudes of the North Atlantic, especially prior to 2050, and part of the salinity increase in subtropics. In contrast, in the North Pacific, while the surface salinity is projected to decrease in  $\Delta$ RCP, there is very little change in  $\Delta$ ICE (not shown), implying the different influences of sea ice loss on the two oceans.

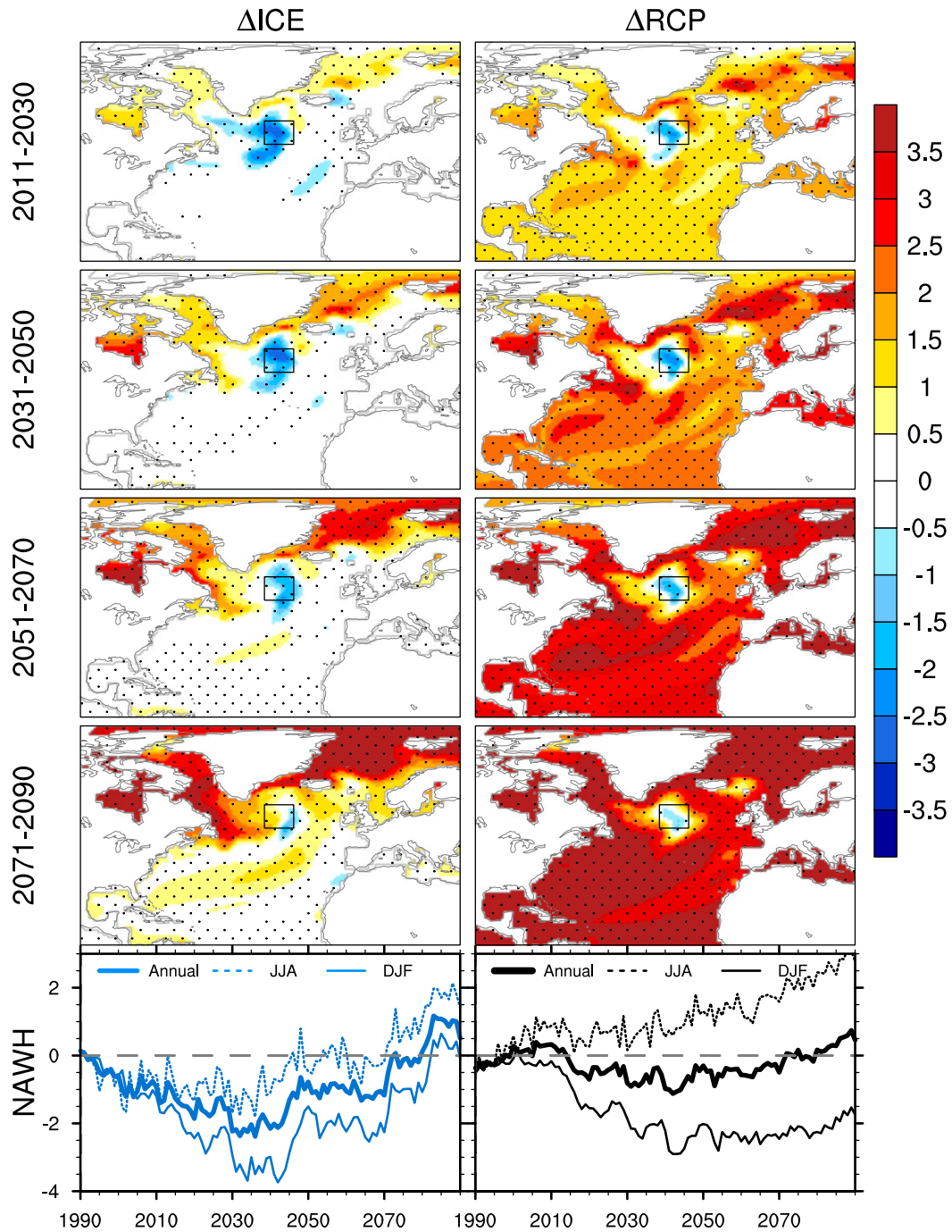


FIG. 5. (top four rows) Annual North Atlantic SST responses in (left)  $\Delta$ ICE and (right)  $\Delta$ RCP averaged over 2011–30, 2031–50, 2051–70, and 2071–90. Black boxes indicate the North Atlantic warming hole (NAWH; 50°–60°N, 27°–37°W). (bottom) Time series of the NAWH annual (thick curve) and JJA and DJF (thin curve) SST responses in (left)  $\Delta$ ICE and (right)  $\Delta$ RCP. Stippling denotes the 95% statistical significance based on two-sided Student's  $t$  test.

*d. NH extratropical atmospheric circulation response*

Figure 7a shows the monthly change of the 700-hPa zonal-mean zonal wind response in  $\Delta$ ICE during 2051–90. The NH atmospheric response peaks in winter

(December–February), characterized by a meridional dipole with zonal wind deceleration centered at 60°N and zonal wind acceleration between 35° and 45°N. There is also zonal wind deceleration at lower latitudes signifying a narrowing of the jet. Figure 7b shows the

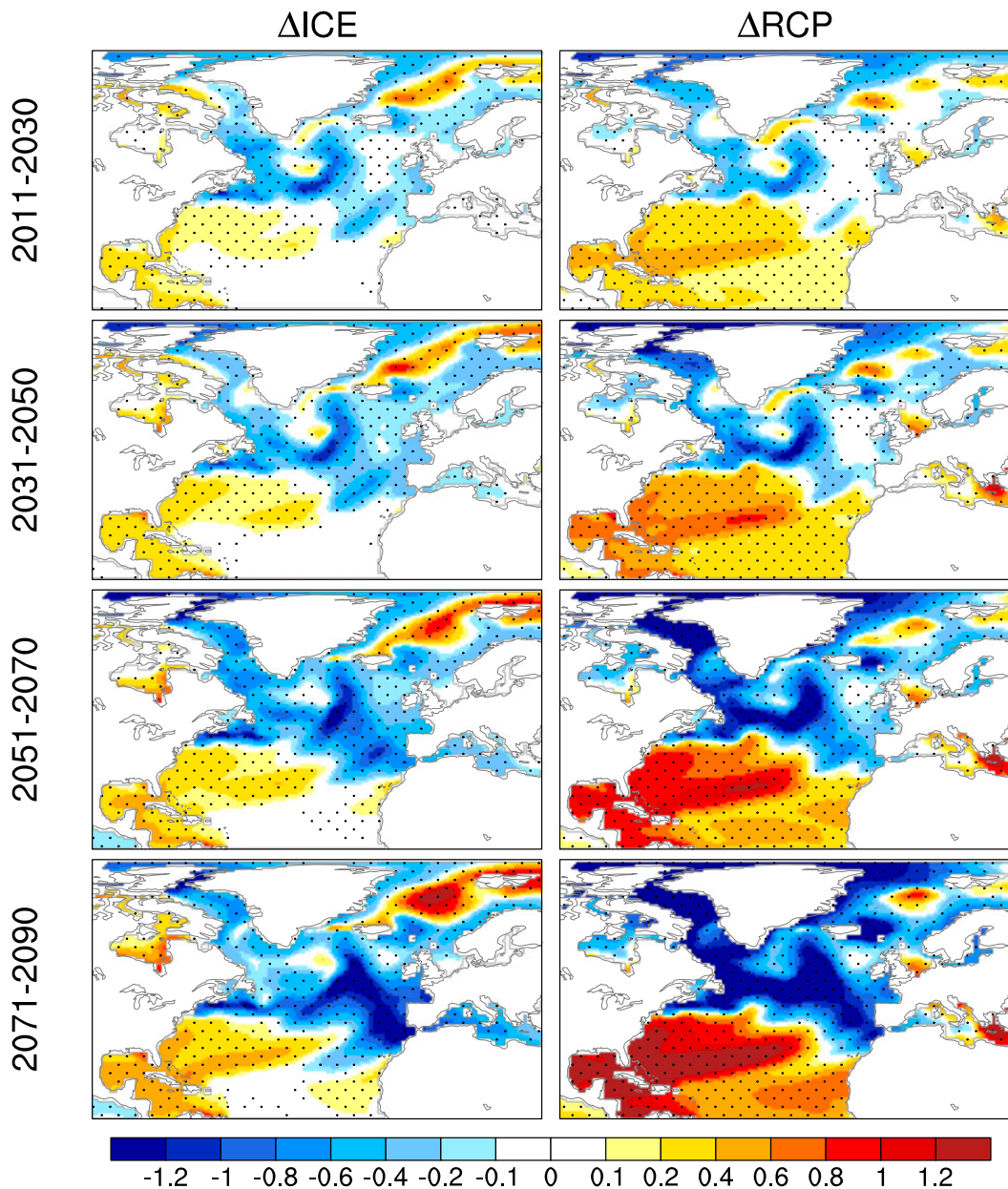


FIG. 6. As in Fig. 5 (top four rows), but for the annual North Atlantic sea surface salinity (SSS; psu) responses in (left)  $\Delta$ ICE and (right)  $\Delta$ RCP averaged over 2011–30, 2031–50, 2051–70, and 2071–90. Stippling denotes the 95% statistical significance based on a two-sided Student's  $t$  test.

winter 700-hPa zonal wind responses in  $\Delta$ ICE and  $\Delta$ RCP poleward of  $23^{\circ}\text{N}$ . Sea ice loss-induced zonal wind deceleration occurs mostly in northern Eurasia and the North Atlantic over the latitude bands of  $50^{\circ}$ – $70^{\circ}\text{N}$ . The overall pattern in  $\Delta$ ICE is similar to other studies (Deser et al. 2016; Oudar et al. 2017; McCusker et al. 2017). By contrast, the NH zonal wind response in  $\Delta$ RCP exhibits two well-defined meridional dipoles, indicating poleward shift of the jets in the Atlantic and Pacific, respectively. Figure 7c shows the time series of

$50^{\circ}$ – $60^{\circ}\text{N}$  averaged zonal-mean zonal wind responses in  $\Delta$ ICE and  $\Delta$ RCP. Even for the five-member ensemble mean, sea ice loss-induced zonal wind deceleration is obscured by internal variability especially in the earlier period. Likewise, the circulation change due to anthropogenic forcing strengthens relative to internal variability over the twenty-first century, and the sign is opposite to the sea ice loss effect (Fig. 7c; black curve).

The 500-hPa geopotential height (Z500) and sea level pressure (SLP) responses in  $\Delta$ ICE and  $\Delta$ RCP during

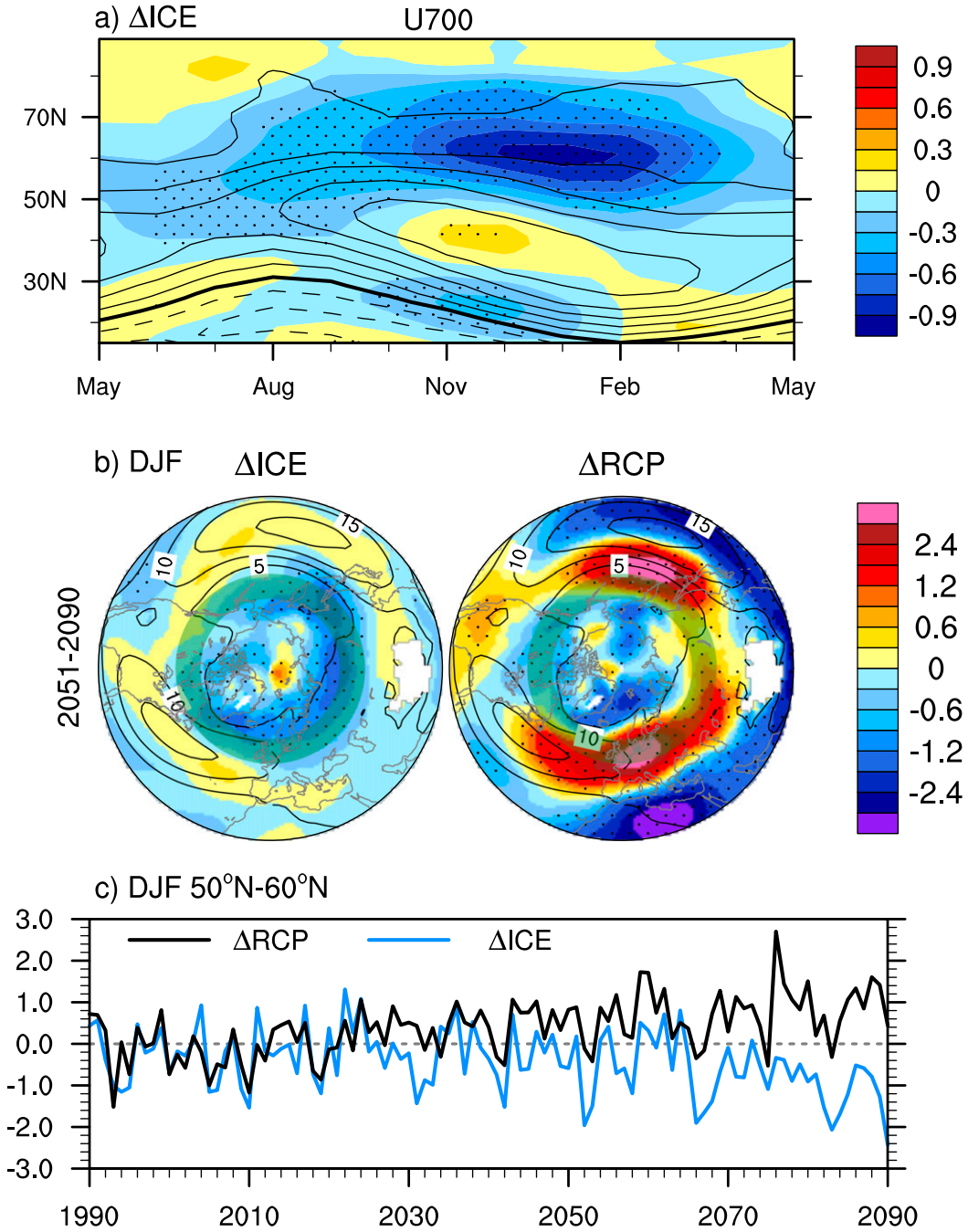
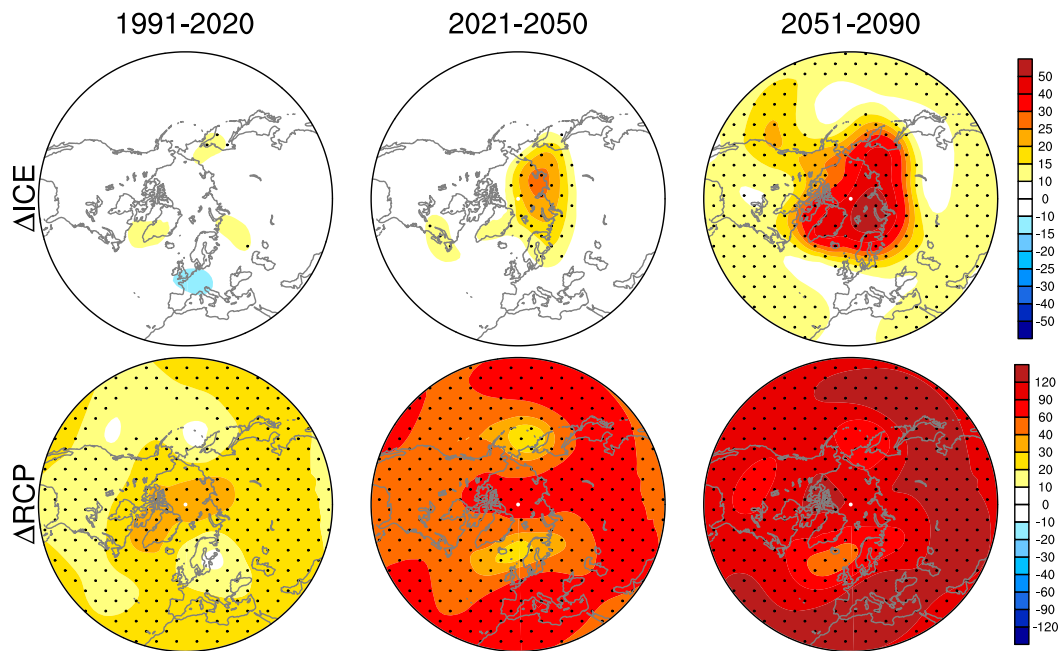


FIG. 7. (a) Monthly change of 700-hPa zonal-mean zonal wind response in  $\Delta\text{ICE}$  averaged over 2051–90. Contours denote the climatology with the interval of  $2 \text{ m s}^{-1}$  and zero wind line thickened. (b) Winter (DJF) 700-hPa zonal wind responses in (left)  $\Delta\text{ICE}$  and (right)  $\Delta\text{RCP}$ . Contours denote the climatology with the interval of  $5 \text{ m s}^{-1}$ . Stippling denotes the 95% statistical significance based on a two-sided Student's  $t$  test. The shading rings indicate the  $50^\circ\text{--}60^\circ\text{N}$  latitude band. (c) Time evolution of winter  $50^\circ\text{--}60^\circ\text{N}$  averaged 700-hPa zonal-mean zonal wind responses in  $\Delta\text{ICE}$  (blue curve) and  $\Delta\text{RCP}$  (black curve).

1991–2020, 2021–50, and 2051–90 are shown in Fig. 8. During 1991–2020, Z500 changes in  $\Delta\text{ICE}$  are mostly less than 10 m and statistically insignificant. During 2021–50 and 2051–90, geopotential height increases over

the polar cap in association with the lower-tropospheric warming in the Arctic, with magnitudes of around 25 and 50 m, respectively. It is distinct from that in  $\Delta\text{RCP}$ , where the height increases everywhere but with smaller

## a) Z3 at 500hPa



## b) Sea-level pressure

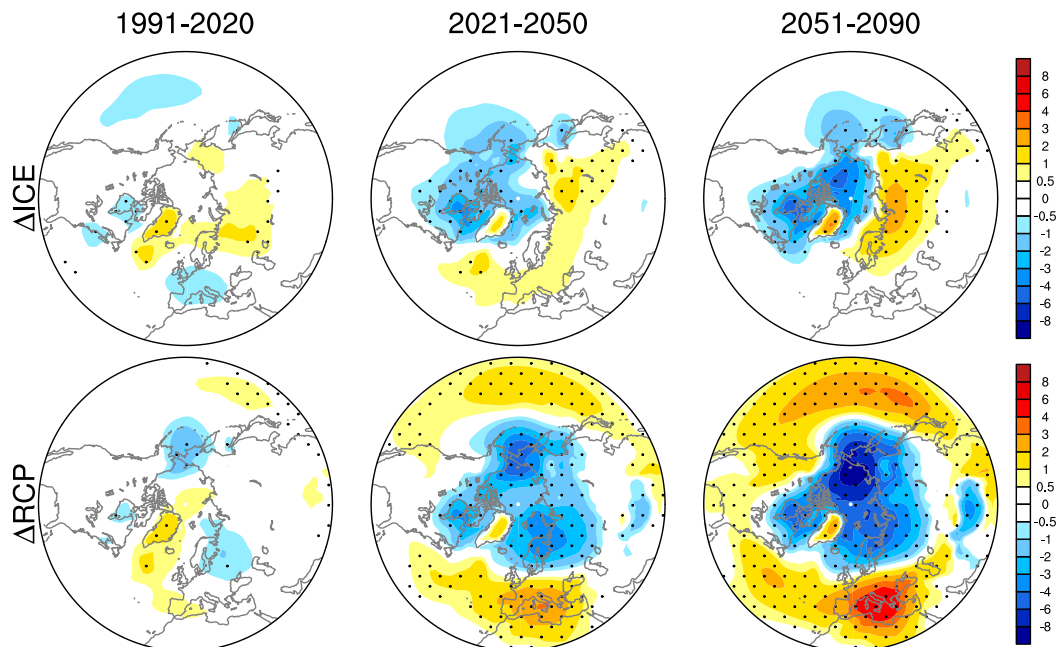


FIG. 8. (a) Winter (DJF) 500-hPa geopotential height (m) responses in  $\Delta$ ICE and  $\Delta$ RCP for 1991–2020, 2021–50, and 2051–90. (b) As in (a), but for the sea level pressure (hPa) responses. Stippling denotes the 95% statistical significance based on a two-sided Student's  $t$  test.

changes over the North Atlantic and North Pacific and greater changes over portions of Eurasia midlatitudes. The magnitude of the Z500 response in  $\Delta$ RCP is always larger than in  $\Delta$ ICE even in the Arctic.

The SLP response in  $\Delta$ ICE during 1991–2020 is weak and there are negative values in the Sea of Okhotsk and Hudson Bay as a result of sea ice loss–induced near-surface warming (Deser et al. 2004). During 2021–50 and

2051–90, sea level pressure change exhibits a well-defined zonal wave-1 pattern with positive values in the Eurasian continent (strengthening of the Siberian high) and negative values in Canada and the North Pacific. This feature has been found to be very robust in both coupled (Deser et al. 2016; Blackport and Kushner 2017; Oudar et al. 2017; McCusker et al. 2017) and uncoupled modeling studies (e.g., Sun et al. 2015; Deser et al. 2016; Semmler et al. 2016). The Aleutian low strengthens in response to Arctic sea ice loss but does not extend as far south in  $\Delta$ ICE as in other coupled model sea ice experiments (Deser et al. 2016; Oudar et al. 2017; McCusker et al. 2017). By contrast, during 2021–50 and 2051–90, sea level pressure in  $\Delta$ RCP is negative over the Arctic and positive over lower latitudes, very different from the sea ice loss effect.

#### e. NH extratropical surface climate response

Figure 9 shows the winter near-surface air temperature and precipitation responses in  $\Delta$ ICE and  $\Delta$ RCP during 1991–2020, 2021–50, and 2051–90. In response to continued Arctic sea ice loss, there is increased warming over high-latitude continents surrounding the ice loss region (i.e., Alaska, northern Canada, Greenland, and northeastern Siberia), and the warming gradually extends to lower latitudes especially in North America. This warming is likely driven by horizontal diffusion (advection by climatological submonthly transient eddies; Deser et al. 2010). There is generally lack of warming in the central/eastern Asia and weak cooling appears in Mongolia (below the smallest interval and statistically insignificant), likely due to cold air advection induced by the enhanced Siberian high (Fig. 8). The overall pattern is robust across models (Screen et al. 2015a; Sun et al. 2015; Deser et al. 2016; Semmler et al. 2016; Blackport and Kushner 2017; Oudar et al. 2017; McCusker et al. 2017) except that the magnitudes vary depending on the interplay between thermodynamic and dynamic effects. The temperature in  $\Delta$ RCP always shows warming with polar amplification.

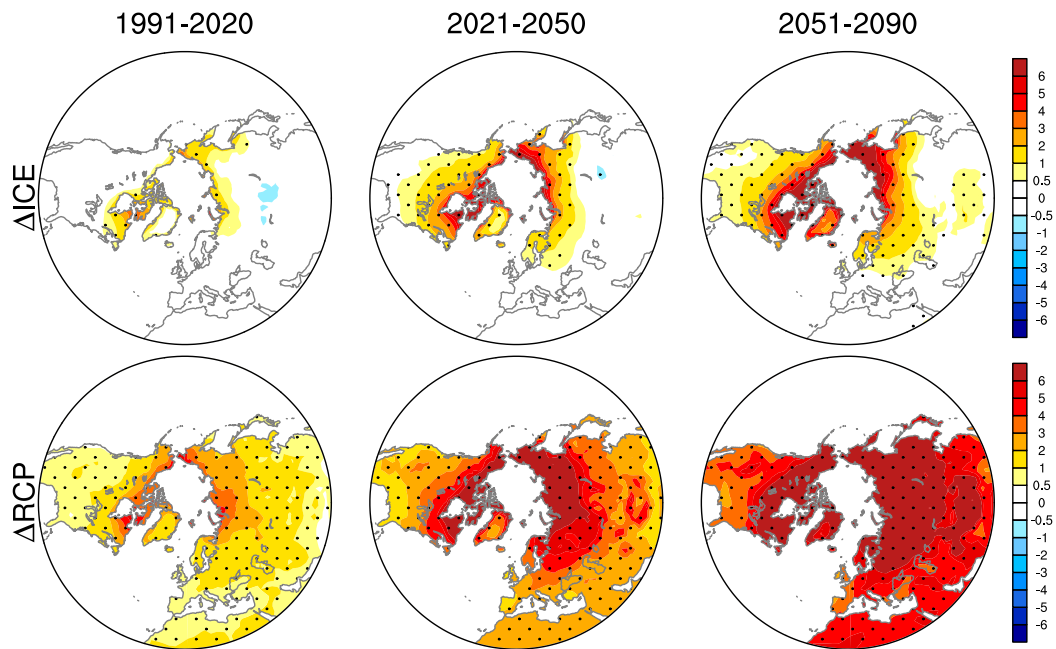
In response to continued sea ice loss the Arctic precipitation increases likely due to enhanced evaporation from the underlying ocean (Fig. S8). The reduction in precipitation over the NAWH is likely related to the negative SSTs and thus less evaporation into the overlying atmosphere (Alexander et al. 2004). In North Pacific and west coast of North America, part of the precipitation increase during 2051–90 may be driven by the deepening Aleutian low (Fig. 8), as also shown in other models (Deser et al. 2016; Hay et al. 2018). The precipitation patterns in  $\Delta$ RCP and  $\Delta$ ICE are similar over the Arctic and the NAWH. However, the mid-latitude signal in  $\Delta$ RCP is much larger and statistically significant especially during 2051–90.

Figure 10a shows  $\Delta$ ICE/ $\Delta$ RCP (in percent) for winter near-surface air temperature response during 2051–90. Over NH high-latitude continents, sea ice loss can explain up to  $\sim$ 80% of the projected temperature increase, while its contribution is generally less than 10% in the subtropics. Similar to Screen et al. (2015b), we select two high-latitude and two midlatitude regions and present the seasonal sea ice loss contributions to the projected near-surface temperature change (Fig. 10b). These four regions are high-latitude North America ( $50^{\circ}$ – $85^{\circ}$ N,  $10^{\circ}$ – $168^{\circ}$ W), high-latitude Eurasia ( $50^{\circ}$ – $85^{\circ}$ N and  $10^{\circ}$ W– $0^{\circ}$ ,  $0^{\circ}$ – $180^{\circ}$ , and  $180^{\circ}$ – $168^{\circ}$ W), western United States (WUS;  $30^{\circ}$ – $50^{\circ}$ N,  $102^{\circ}$ – $120^{\circ}$ W), and eastern United States (EUS;  $30^{\circ}$ – $50^{\circ}$ N;  $60^{\circ}$ – $102^{\circ}$ W), respectively. In all four regions the sea ice loss contribution is largest during winter and smallest during summer, consistent with the surface energy flux response (Fig. 2a). Over high latitudes, a larger winter sea ice contribution occurs in North America ( $\sim$ 55%) than in Eurasia (30%). In the eastern United States, the winter sea ice loss contribution reaches more than 30%, significantly larger than over the western United States. This is likely because Hudson Bay resides at a relatively low latitude (the south edge is at  $\sim$ 50°N). Therefore, the local warming associated with the sea ice loss can more effectively warm the land farther south, especially during cold days when the winds are blowing from the north (Screen 2014). The role of the Arctic sea ice loss in causing eastern North American warming and reducing cold extremes can be seen in other studies (e.g., Screen et al. 2015a; Sun et al. 2015; Blackport and Kushner 2017; Deser et al. 2016; Sun et al. 2016; McCusker et al. 2017). The evolution of the fraction  $\Delta$ ICE/ $\Delta$ RCP is shown in Fig. 10c, with temporal smoothing to reduce the influence of internal variability. While all of the NH extratropical regions warm in both  $\Delta$ ICE and  $\Delta$ RCP, the sea ice contribution to the warming remains nearly constant over time except in the high-latitude North America where the fraction increases by  $\sim$ 10% during 2010–70 (and likely related to the ice loss mismatch between  $\Delta$ ICE and  $\Delta$ RCP).

#### f. Tropical climate response

Arctic sea ice loss can drive tropical SST and precipitation changes remotely through several processes including a decline in AMOC (Zhang and Delworth 2005) and atmosphere–ocean thermodynamical coupling (e.g., Chiang and Bitz 2005), or both (Tomas et al. 2016). Figure 11 shows annual SST and precipitation responses in  $\Delta$ ICE and  $\Delta$ RCP during 2051–90 (note that difference color scales have been used because the SST response in  $\Delta$ ICE is much smaller than in  $\Delta$ RCP). Although  $\Delta$ ICE only accounts for  $\sim$ 10% of the SST responses in  $\Delta$ RCP when zonally averaged, the

### a) Near-surface air temperature



### b) Precipitation

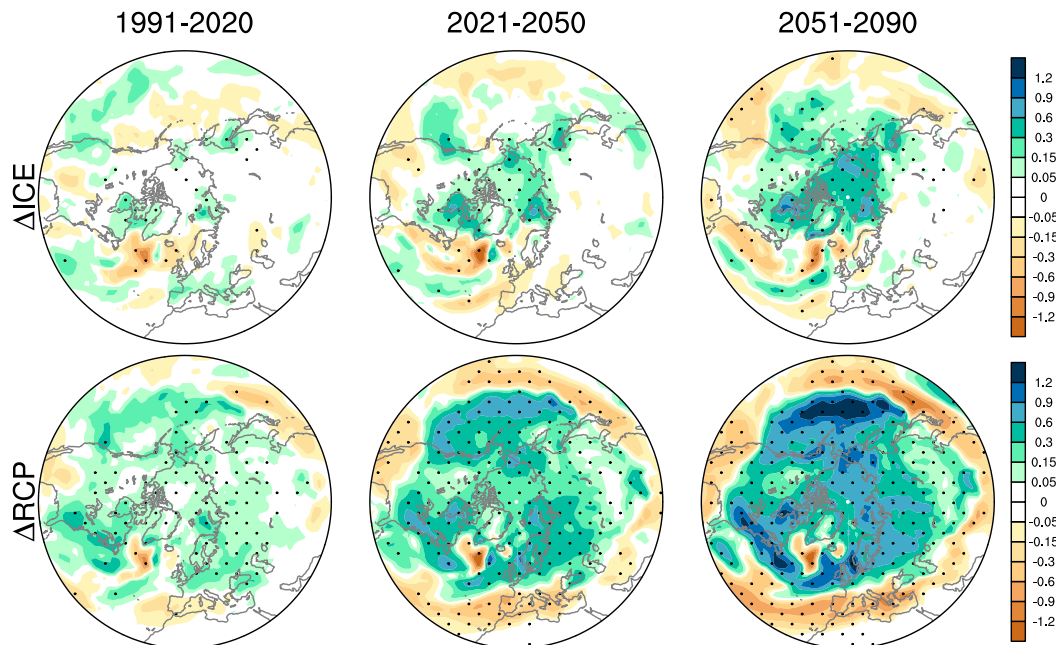


FIG. 9. As in Fig. 8, but for (a) near-surface air temperature ( $^{\circ}\text{C}$ ) and (b) precipitation ( $\text{mm day}^{-1}$ ) responses in  $\Delta\text{ICE}$  and  $\Delta\text{RCP}$  for 1991–2020, 2021–50, and 2051–90. Stippling denotes the 95% statistical significance based on a two-sided Student's  $t$  test.

features are similar, with a pattern correlation of 0.76 in the tropics. For example, SST responses in  $\Delta\text{ICE}$  and  $\Delta\text{RCP}$  both exhibit enhanced warming along the equator in the central and eastern Pacific.

In response to Arctic sea ice loss, the tropical Pacific precipitation increases on the equatorward side of the climatological ITCZ in both hemispheres. In the tropical Atlantic, the ITCZ strengthens, while in the Indian

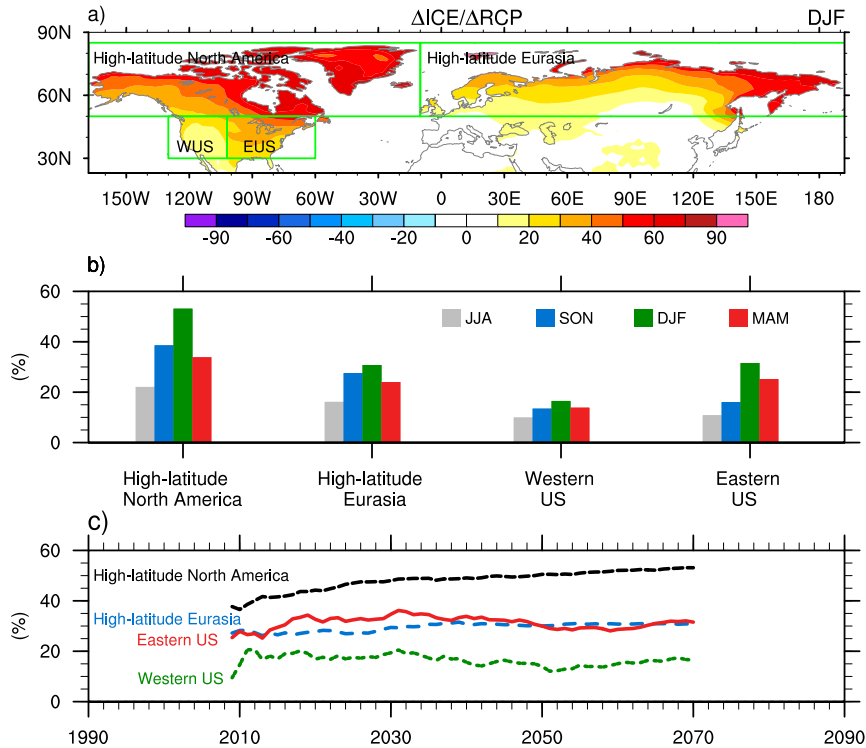


FIG. 10. (a) Fraction (%) of  $\Delta\text{ICE}/\Delta\text{RCP}$  for winter near-surface air temperature response in 2051–90. Green boxes denote various high-latitude and midlatitude continents, including high-latitude North America, high-latitude Eurasia, western United States (WUS), and eastern United States (EUS). (b) As in (a), but averaged over four individual continents in JJA (gray bars), SON (light blue bars), DJF (green bars), and MAM (red bars). (c) As in (b), but for the time evolution of winter temperature response fractions. To remove the internal variability, 40-yr running mean is first performed before calculating the fraction.

Ocean precipitation increases on the north side of the equator, indicating a northward shift of the ITCZ. These features in  $\Delta\text{ICE}$  are largely similar to  $\Delta\text{RCP}$  (Fig. 11b), despite the fact that it only accounts for  $\sim 16\%$  of the total anthropogenic change over  $15^{\circ}\text{S}$ – $15^{\circ}\text{N}$ .

Figure 12 shows the evolution of the zonal-mean annual tropical SST and precipitation responses in  $\Delta\text{ICE}$  and  $\Delta\text{RCP}$ , after applying a 30-yr running mean to reduce the influence of internal variability. The tropical response to transient Arctic sea ice loss is characterized by SST warming from  $\sim 0.02^{\circ}\text{C}$  around 2020 to  $\sim 0.3^{\circ}\text{C}$  by 2070. Associated with the SST change, precipitation increases at  $5^{\circ}\text{S}$ – $10^{\circ}\text{N}$  with the peak at  $\sim 7^{\circ}\text{N}$ , ranging from  $\sim 0.015\text{ mm day}^{-1}$  in 2010 to  $\sim 0.24\text{ mm day}^{-1}$  in 2070. Precipitation initially decreases in the latitude bands of  $10^{\circ}$ – $20^{\circ}\text{N}$  and  $5^{\circ}$ – $20^{\circ}\text{S}$ , but the NH drying zone gradually decreases and disappears by  $\sim 2070$ . The evolutions of SST and precipitation responses in  $\Delta\text{RCP}$  are similar to sea ice loss effect, but the magnitude is much larger. In  $\Delta\text{RCP}$ , precipitation increases over  $5^{\circ}\text{S}$ – $20^{\circ}\text{N}$  peaking at  $\sim 7^{\circ}\text{N}$ , but extending farther northward

than in  $\Delta\text{ICE}$ . Similar to  $\Delta\text{ICE}$ , there is also a drying zone south of  $5^{\circ}\text{S}$  in  $\Delta\text{RCP}$ . Moreover, when averaged over the tropics, the sea ice loss contribution to the total anthropogenic climate change appears to gradually increase with time for both SST and precipitation (Fig. S9), suggesting that the tropical response takes more time to emerge than high-latitude response.

Figure 13 presents the zonal-mean annual temperature and zonal-wind responses as a function of pressure and latitude in  $\Delta\text{ICE}$  and  $\Delta\text{RCP}$  during 2051–90. In response to the sea ice loss, strong near-surface warming occurs in the Arctic, accounting for most of the projected RCP change (also see Fig. 3a). A weak warming of  $\sim 0.7^{\circ}\text{C}$  can also be observed in the tropical upper troposphere, in association with enhanced equatorial convection and latent heat release. While  $\Delta\text{ICE}$  only explains  $\sim 8\%$  of the tropical tropospheric temperature signal in  $\Delta\text{RCP}$ , it is statistically significant and robust across all five members (not shown). This so-called “mini-global warming” (Deser et al. 2015) has been found to be robust among different coupled ocean–atmosphere

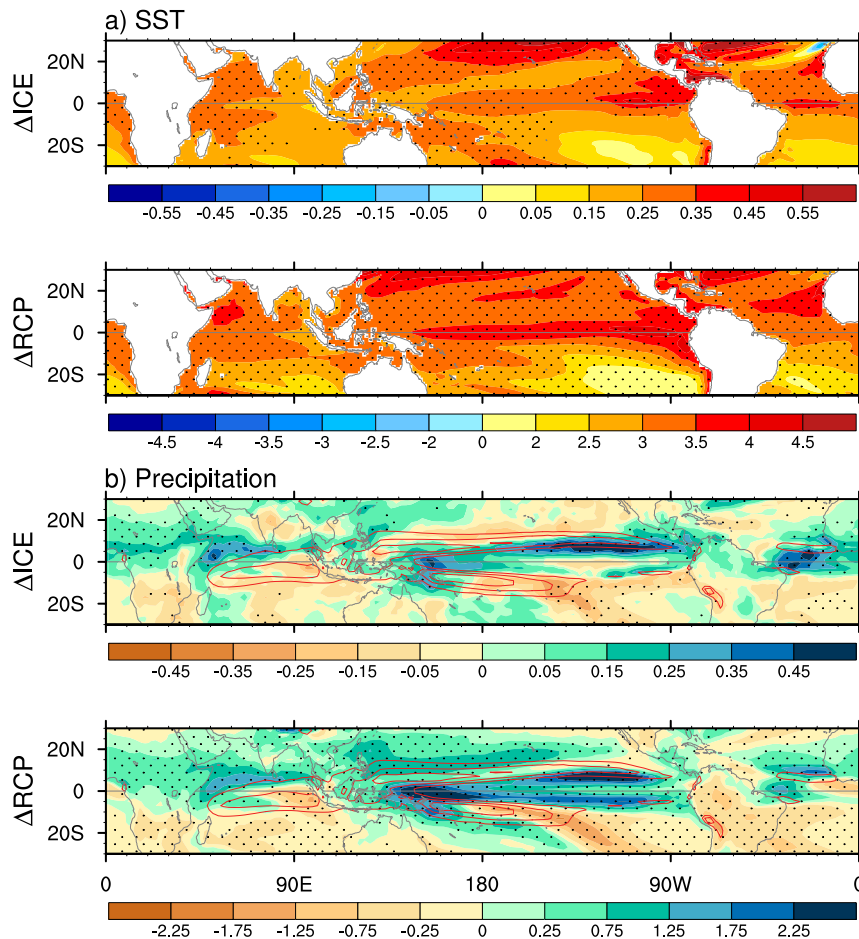


FIG. 11. (a): Annual tropical SST ( $^{\circ}\text{C}$ ) response in  $\Delta\text{ICE}$  and  $\Delta\text{RCP}$  averaged over 2051–90. (b) As in (a), but for precipitation ( $\text{mm day}^{-1}$ ) response, overlaid by its climatology. Stippling denotes the 95% statistical significance based on a two-sided Student's  $t$  test.

modeling studies (Screen et al. 2018). The zonal wind response to Arctic sea ice loss is largely consistent with the temperature response via the thermal wind relationship. The westerly winds weaken over NH high latitudes centered at  $60^{\circ}\text{N}$ , in contrast to the meridional dipole in  $\Delta\text{RCP}$ , as already shown at 700 hPa (Fig. 7b). The westerly winds are strengthened in the subtropical upper troposphere and lower stratosphere in both hemispheres, in response to the tropical upper-tropospheric warming.

#### 4. Summary and discussion

##### a. Summary

In this study, we use GFDL's coupled ocean–atmosphere model CM3 to evaluate the role of transient Arctic sea ice loss in the projected GHG-induced global climate change from the late twentieth century to

the late twenty-first century. Our key findings are summarized as follows.

- 1) Within the Arctic, sea ice loss is the primary driver of climate change, especially for sea surface temperature and near-surface air temperature. The sea ice contribution to total climate change is very similar for 2011–50 and 2050–90. The increase in total precipitation is closely related to sea ice depletion in winter but not in summer.
- 2) Arctic sea ice loss is one crucial factor for AMOC weakening and the formation of the “North Atlantic warming hole.” Roughly half of the projected AMOC decline in twenty-first century due to anthropogenic forcing can be attributed to the loss of sea ice, and its contribution is even larger for the present day and the near future, although part of the rapid change may come from natural variability. Associated with the AMOC change, the North

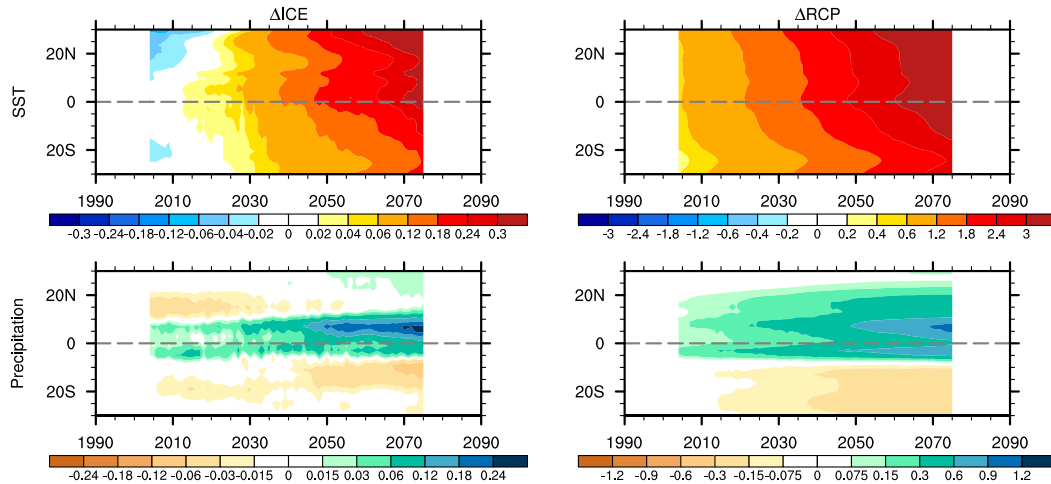


FIG. 12. (top) Annual tropical zonal-mean SST ( $^{\circ}\text{C}$ ) response as a function of time and latitude in (left)  $\Delta\text{ICE}$  and (right)  $\Delta\text{RCP}$ . (bottom) As in (top), but for annual tropical zonal-mean precipitation ( $\text{mm day}^{-1}$ ) response. To remove internal variability, SST and precipitation responses have been smoothed by 30-yr running mean. Note that the color scales are different between  $\Delta\text{ICE}$  and  $\Delta\text{RCP}$ .

Atlantic warming hole appears with respect to the climatology. The cooling is stronger in winter than in summer. Moreover, the freshening of the North Atlantic subpolar gyre caused by sea ice loss can explain most of the projected salinity change, especially prior to 2050. Sea ice loss-induced surface salinity also increases in North Atlantic subtropical

gyre, albeit with a smaller contribution than in the subpolar gyre.

3) In contrast to the AMOC adjustment, the NH atmospheric circulation response to present-day Arctic sea ice loss is small relative to internal variability. There is little signal in wind, sea level pressure, and geopotential height prior to 2020 even

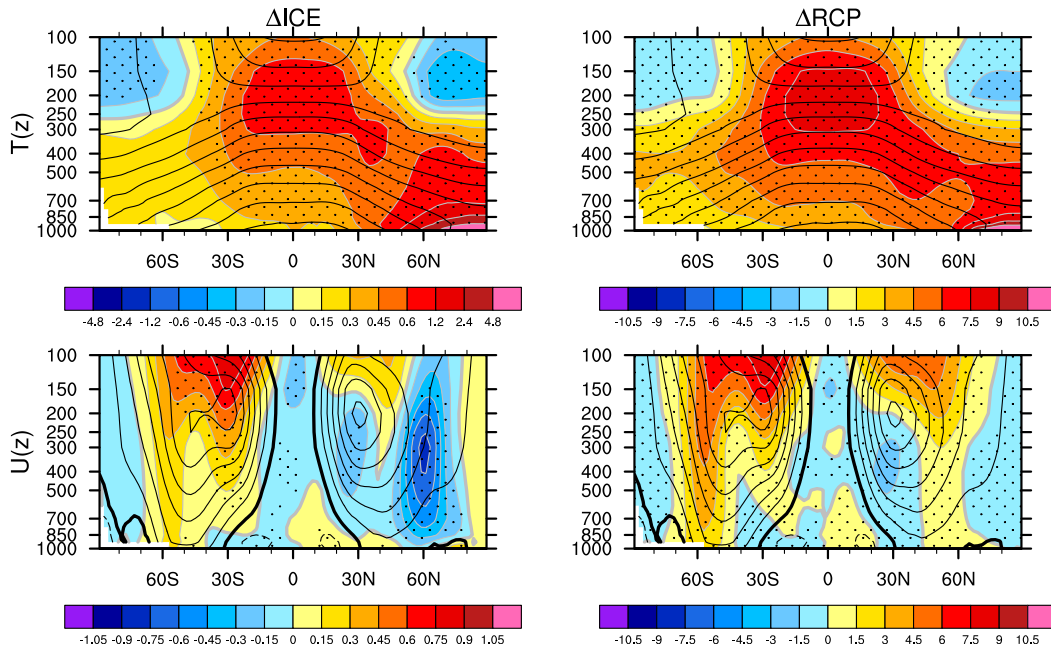


FIG. 13. (top) Annual zonal-mean temperature ( $^{\circ}\text{C}$ ) response in (left)  $\Delta\text{ICE}$  and (right)  $\Delta\text{RCP}$  averaged over 2051–90, overlaid by the climatology (contours). The contour interval is  $10^{\circ}\text{C}$ . (bottom) As in (top), but for zonal-mean zonal wind ( $\text{m s}^{-1}$ ) response. Contour interval is  $5 \text{ m s}^{-1}$ . Stippling denotes the 95% statistical significance based on a two-sided Student's  $t$  test.

though the simulated sea ice reduction is slightly larger than in observations. The sea ice loss effect on the atmospheric circulation is distinct from the projected anthropogenic change, suggesting that the circulation change initiated from the Arctic is small relative to changes in other parts of the climate system (e.g., tropical SSTs) due to an increase in greenhouse gases.

- 4) Arctic sea ice loss warms the NH extratropical continents over the course of the twenty-first century. It is an important contributor to greenhouse gas-induced increases in surface air temperature not only at high latitudes, but also over the eastern United States. While temperatures continue to increase over the NH continents due to anthropogenic forcing, the sea ice contribution remains nearly constant with time.
- 5) Arctic sea ice loss can remotely influence the tropical SST and precipitation, causing an equatorward displacement of the Pacific ITCZ. This effect is small but robust, and is similar to the RCP change. Associated with the precipitation increase in the deep tropics, there is a “mini-global warming” response to continued Arctic sea ice loss.

The response at the end of the twenty-first century in our transient sea ice loss experiments is in general agreement with the equilibrium responses to an abrupt loss of late-twenty-first-century Arctic sea ice (e.g., Deser et al. 2015, 2016; Blackport and Kushner 2016, 2017; Oudar et al. 2017; McCusker et al. 2017). This implies that these equilibrium responses provide a reasonable representation of end-of-century impacts of sea ice loss. Moreover, our experimental design provides additional information on the climatic impacts of a transitioning sea ice cover. We find that for many fields, the response increases approximately linearly with time over the course of the twenty-first century. A notable exception is the AMOC response, which exhibits nonlinear behavior for reasons that remain to be understood.

### *b. Discussion*

The results presented above highlight a number of issues. The first issue concerns the evolution of the AMOC response. In our experiments, we found that Arctic sea ice loss induces significant weakening of AMOC over the first two decades of the experiment, consistent with other recent studies (Blackport and Kushner 2016; Tomas et al. 2016; Oudar et al. 2017; Sévellec et al. 2017). Thus, the recent loss of sea ice may have already affected the ocean circulation. This is in contrast to the sea ice loss-induced atmospheric circulation

response, which still exhibits low detectability due to high internal variability (e.g., Screen et al. 2014; Smith et al. 2017). The processes responsible for the AMOC response, in particular the role of surface heat versus freshwater flux in causing AMOC to weaken, need further investigation.

While the AMOC slowdown is a common feature of various sea ice experiments with fully coupled ocean–atmosphere models, the changes of AMOC time series and the contribution of sea ice loss differ across models. For example, in Blackport and Kushner (2016) AMOC declines in the first several decades but then recovers over the following ~400 years, whereas in Deser et al. (2015) and Oudar et al. (2017) AMOC is in quasi-equilibrium after its initial slowdown without a clear indication of recovery. The contribution of sea ice loss to AMOC decline in full climate change simulations is found also to differ; for example, the decline is ~30% in Tomas et al. (2016), 75% in Sévellec et al. (2017), and more than 100% in Oudar et al. (2017). Differences can arise due to many factors, such as the methodology used in the sea ice experiments, abrupt versus transient sea ice loss, and the magnitude of the sea ice change. Moreover, the percentage of sea ice contribution varies when looking at the early versus the late twenty-first century; in our study, it is found to be much larger in the earlier period, which highlights the unique value of the transient sea ice experiments.

The second issue concerns the atmospheric response to Arctic sea ice loss over time. While the atmospheric circulation response to late-twenty-first-century Arctic sea ice loss has been found to be robust across models (Screen et al. 2018), the response to present-day sea ice loss differs between modeling studies (e.g., Mori et al. 2014; Kim et al. 2014; Perlwitz et al. 2015; McCusker et al. 2016; Sun et al. 2016). The transient experiments performed here may help to explain this transition. During 2051–90, the sea ice loss effect is qualitatively in agreement with previous studies (Deser et al. 2015; Blackport and Kushner 2016, 2017; Oudar et al. 2017; McCusker et al. 2017; Hay et al. 2018). During 1991–2020, however, the atmospheric circulation response to sea ice loss is very weak and statistically insignificant (Figs. 7 and 8), even though the sea ice reduction in CM3 is slightly larger than in observations (Fig. 1b). Thus, a very large number of samples are probably needed in order to evaluate the effects of Arctic sea ice loss and it might not be possible to disentangle the impact of sea ice loss from other effects based on a short period of observations (Smith et al. 2017). In addition, the surface air temperature response in our experiments is in agreement with other coupled and uncoupled model studies (Screen et al. 2015a; Sun et al. 2015; Deser et al. 2016;

Semmler et al. 2016; Blackport and Kushner 2017; Oudar et al. 2017; McCusker et al. 2017, Hay et al. 2018), suggesting that sea ice loss makes a substantial contribution to warming in the eastern United States, rather than cooling due to changes in atmospheric dynamics (e.g., Francis et al. 2017).

A related issue is that while the future sea ice loss effect is generally found to be robust across models, the atmospheric circulation response to total anthropogenic forcing is more model dependent. For example, some models exhibit a meridional dipole with zonal wind strengthening at the latitude band of 20°–40°N and weakening centered around 60°N (Oudar et al. 2017; McCusker et al. 2017), while others do not show a clear zonal-mean jet change (Deser et al. 2015; Blackport and Kushner 2017), both different from the poleward jet shift found in our ice loss experiments. The diversity of climate change responses among models might reflect different balances in the “tug of war” between tropical warming and Arctic warming (e.g., Barnes and Polvani 2015; Deser et al. 2015; Blackport and Kushner 2017; McCusker et al. 2017; Oudar et al. 2017) or differences in the circulation response to tropical forcing (Hay et al. 2018).

The last issue concerns the processes by which Arctic sea ice influences the Pacific ITCZ, or more broadly, how the high-latitude forcing impacts the tropical SST and precipitation. Our results are largely in agreement with those of Deser et al. (2015), who used CCSM4, which includes a dynamical ocean model, and differs from studies using slab ocean models (e.g., Chiang and Bitz 2005; Broccoli et al. 2006; Kang et al. 2008; Frierson and Hwang 2012; Cvijanovic et al. 2017) or a fully coupled model but with constraining temperature and salinity below 200 m (Smith et al. 2017). Although we have not examined the global energy balance in our experiments, we speculate that poleward oceanic heat transport is the key to understanding the difference between our results and those of previous slab-ocean coupled modeling studies, consistent with the findings of Tomas et al. (2016). In particular, without ocean dynamics, Arctic sea ice loss results in a reduction of atmospheric northward heat transport (NHT) across the equator and thus shifts the ITCZ northward; with ocean dynamics, both oceanic and atmospheric NHT diminish in response to Arctic sea ice loss (Deser et al. 2015; Tomas et al. 2016). As suggested by Cabré et al. (2017), the tropical ITCZ response to high-latitude forcing might depend on the partitioning between atmospheric and oceanic components of the cross-equator energy transport. We note that the tropical upper-tropospheric warming associated with future sea ice loss has also been found in other fully

coupled experiments (Screen et al. 2018), suggesting that the so-called mini-global warming is a common feature among models in response to Arctic sea ice loss.

To what extent our results are model dependent remains to be ascertained. The upcoming CMIP6 Polar Amplification Model Intercomparison Project (PAMIP) should be helpful in this regard, as all models will follow the same experimental protocol (Smith et al. 2018). In future work, we plan to investigate the mechanisms underlying the nonlinear AMOC response to transient Arctic sea ice loss, as well as the subseasonal atmospheric response including storm-track metrics and climate extremes.

*Acknowledgments.* We thank Tom Knutson, Rong Zhang, Michael Winton, and Fanrong Zeng at GFDL for help in setting up the model experiments and valuable discussions, and Martin Hoerling and Judith Perlwitz at ESRL/PSD for their constructive suggestions. We also thank the three anonymous reviewers and Editor John Chiang for their helpful and constructive comments. This project was supported by the NOAA Climate Program Office Earth System Modeling program. NCAR is sponsored by the National Science Foundation.

## REFERENCES

- Alexander, M. A., U. S. Bhatt, J. E. Walsh, M. S. Timlin, J. S. Miller, and J. D. Scott, 2004: The atmospheric response to realistic Arctic sea ice anomalies in an AGCM during winter. *J. Climate*, **17**, 890–905, [https://doi.org/10.1175/1520-0442\(2004\)017<0890:TARTRA>2.0.CO;2](https://doi.org/10.1175/1520-0442(2004)017<0890:TARTRA>2.0.CO;2).
- , J. D. Scott, K. D. Friedland, K. E. Mills, J. A. Nye, A. J. Pershing, and A. C. Thomas, 2018: Projected sea surface temperatures over the 21st century: Changes in the mean, variability and extremes for large marine ecosystem regions of northern oceans. *Elementa Sci. Anthropocene*, **6**, 9, <https://doi.org/10.1525/elementa.191>.
- Andrews, T., J. M. Gregory, M. J. Webb, and K. E. Taylor, 2012: Forcing, feedbacks and climate sensitivity in CMIP5 coupled atmosphere–ocean climate models. *Geophys. Res. Lett.*, **39**, L09712, <https://doi.org/10.1029/2012GL051607>.
- Barnes, E. A., and L. Polvani, 2015: CMIP5 projections of Arctic amplification, of the North American/North Atlantic circulation, and of their relationship. *J. Climate*, **28**, 5254–5271, <https://doi.org/10.1175/JCLI-D-14-00589.1>.
- , and J. A. Screen, 2015: The impact of Arctic warming on the midlatitude jet-stream: Can it? Has it? Will it? *Wiley Interdiscip. Rev.: Climate Change*, **6**, 277–286, <https://doi.org/10.1002/wcc.337>.
- Bintanja, R., and O. Andry, 2017: Towards a rain-dominated Arctic. *Nat. Climate Change*, **7**, 263–267, <https://doi.org/10.1038/nclimate3240>.
- Bitz, C. M., P. R. Gent, R. A. Woodgate, M. M. Holland, and R. Lindsay, 2006: The influence of sea ice on ocean heat

- uptake in response to increasing CO<sub>2</sub>. *J. Climate*, **19**, 2437–2450, <https://doi.org/10.1175/JCLI3756.1>.
- Blackport, R., and P. Kushner, 2016: The transient and equilibrium climate response to rapid summertime sea ice loss in CCSM4. *J. Climate*, **29**, 401–417, <https://doi.org/10.1175/JCLI-D-15-0284.1>.
- , and —, 2017: Isolating the atmospheric circulation response to Arctic sea ice loss in the coupled climate system. *J. Climate*, **30**, 2163–2185, <https://doi.org/10.1175/JCLI-D-16-0257.1>.
- Broccoli, A. J., K. A. Dahl, and R. J. Stouffer, 2006: Response of the ITCZ to Northern Hemisphere cooling. *Geophys. Res. Lett.*, **33**, L01702, <https://doi.org/10.1029/2005GL024546>.
- Cabr , A., I. Marinov, and A. Gnanadesikan, 2017: Global atmospheric teleconnections and multidecadal climate oscillations driven by Southern Ocean convection. *J. Climate*, **30**, 8107–8126, <https://doi.org/10.1175/JCLI-D-16-0741.1>.
- Caesar, L., S. Rahmstorf, A. Robinson, G. Feulner, and V. Saba, 2018: Observed fingerprint of a weakening Atlantic Ocean overturning circulation. *Nature*, **556**, 191–196, <https://doi.org/10.1038/s41586-018-0006-5>.
- Cheng, W., J. C. Chiang, and D. Zhang, 2013: Atlantic meridional overturning circulation (AMOC) in CMIP5 models: RCP and historical simulations. *J. Climate*, **26**, 7187–7197, <https://doi.org/10.1175/JCLI-D-12-00496.1>.
- Chiang, J. C. H., and C. M. Bitz, 2005: Influence of high latitude ice on the marine intertropical convergence zone. *Climate Dyn.*, **25**, 477–496, <https://doi.org/10.1007/s00382-005-0040-5>.
- Collins, M., and Coauthors, 2013: Long-term climate change: Projections, commitments and irreversibility. *Climate Change 2013: The Physical Science Basis*, T. F. Stocker et al., Eds., Cambridge University Press, 1029–1136, <https://doi.org/10.1017/CBO9781107415324.024>.
- Cvijanovic, I., B. Santer, C. Bonfils, D. D. Lucas, J. C. H. Chiang, and S. Zimmerman, 2017: Future loss of Arctic sea-ice cover could drive a substantial decrease in California’s rainfall. *Nat. Commun.*, **8**, 1947, <https://doi.org/10.1038/s41467-017-01907-4>.
- Day, J. J., J. C. Hargreaves, J. D. Annan, and A. Abe-Ouchi, 2012: Sources of multi-decadal variability in Arctic sea ice extent. *Environ. Res. Lett.*, **7**, 034011, <https://doi.org/10.1088/1748-9326/7/3/034011>.
- Delworth, T. L., and Coauthors, 2006: GFDL’s CM2 global coupled climate models. Part I: Formulation and simulation characteristics. *J. Climate*, **19**, 643–674, <https://doi.org/10.1175/JCLI3629.1>.
- Deser, C., G. Magnusdottir, R. Saravanan, and A. Phillips, 2004: The effects of North Atlantic SST and sea-ice anomalies on the winter circulation in CCM3. Part II: Direct and indirect components of the response. *J. Climate*, **17**, 877–889, [https://doi.org/10.1175/1520-0442\(2004\)017<0877:TEONAS>2.0.CO;2](https://doi.org/10.1175/1520-0442(2004)017<0877:TEONAS>2.0.CO;2).
- , R. A. Tomas, M. A. Alexander, and D. Lawrence, 2010: The seasonal atmospheric response to projected Arctic sea ice loss in the late twenty-first century. *J. Climate*, **23**, 333–351, <https://doi.org/10.1175/2009JCLI3053.1>.
- , —, and L. Sun, 2015: The role of ocean–atmosphere coupling in the zonal-mean atmospheric response to Arctic sea ice loss. *J. Climate*, **28**, 2168–2186, <https://doi.org/10.1175/JCLI-D-14-00325.1>.
- , L. Sun, R. A. Tomas, and J. Screen, 2016: Does ocean coupling matter for the northern extratropical response to projected Arctic sea ice loss? *Geophys. Res. Lett.*, **43**, 2149–2157, <https://doi.org/10.1002/2016GL067792>.
- Ding, Q., and Coauthors, 2017: Influence of high-latitude atmospheric circulation changes on summertime Arctic sea ice. *Nat. Climate Change*, **7**, 289–295, <https://doi.org/10.1038/nclimate3241>.
- Donner, L. J., and Coauthors, 2011: The dynamical core, physical parameterizations, and basic simulation characteristics of the atmospheric component of the GFDL global coupled model CM3. *J. Climate*, **24**, 3484–3519, <https://doi.org/10.1175/2011JCLI3955.1>.
- Fetterer, F., K. Knowles, W. Meier, M. Savoie, and A. K. Windnagel, 2017 (updated daily): Sea Ice Index, version 3 [Arctic sea ice extent]. National Snow and Ice Data Center, <https://doi.org/10.7265/N5K072F8>.
- Francis, J. A., S. J. Vavrus, and J. Cohen, 2017: Amplified Arctic warming and mid-latitude weather: New perspectives on emerging connections. *Wiley Interdiscip. Rev.: Climate Change*, **8**, e474, <https://doi.org/10.1002/wcc.474>.
- Frierson, D. M. W., and Y.-T. Hwang, 2012: Extratropical influence on ITCZ shifts in slab ocean simulations of global warming. *J. Climate*, **25**, 720–733, <https://doi.org/10.1175/JCLI-D-11-00116.1>.
- Golaz, J.-C., M. Salzmann, L. J. Donner, L. W. Horowitz, Y. Ming, and M. Zhao, 2011: Sensitivity of the aerosol indirect effect to subgrid variability in the cloud parameterization of the GFDL atmosphere general circulation model AM3. *J. Climate*, **24**, 3145–3160, <https://doi.org/10.1175/2010JCLI3945.1>.
- Graversen, R. G., and M. Wang, 2009: Polar amplification in a coupled climate model with locked albedo. *Climate Dyn.*, **33**, 629–643, <https://doi.org/10.1007/s00382-009-0535-6>.
- Griffies, S. M., and Coauthors, 2011: GFDL’s CM3 coupled climate model: Characteristics of the ocean and sea ice simulations. *J. Climate*, **24**, 3520–3544, <https://doi.org/10.1175/2011JCLI3964.1>.
- Hay, S., P. Kushner, R. Blackport, and K. McCusker, 2018: On the relative robustness of the atmospheric circulation response to high-latitude and low-latitude warming. *Geophys. Res. Lett.*, **45**, 6232–6241, <https://doi.org/10.1029/2018GL077294>.
- Jahn, A., J. E. Kay, M. M. Holland, and D. M. Hall, 2016: How predictable is the timing of a summer ice-free Arctic? *Geophys. Res. Lett.*, **43**, 9113–9120, <https://doi.org/10.1002/2016GL070067>.
- Kang, S. M., I. M. Held, D. M. W. Frierson, and M. Zhao, 2008: The response of the ITCZ to extratropical thermal forcing: Idealized slab-ocean experiments with a GCM. *J. Climate*, **21**, 3521–3532, <https://doi.org/10.1175/2007JCLI2146.1>.
- Kay, J. E., C. Wall, V. Yettella, B. Medeiros, C. Hannay, P. Caldwell, and C. Bitz, 2016: Global climate impacts of fixing the Southern Ocean shortwave radiation bias in the Community Earth System Model (CESM). *J. Climate*, **29**, 4617–4636, <https://doi.org/10.1175/JCLI-D-15-0358.1>.
- Kim, B.-M., S.-W. Son, S.-K. Min, J.-H. Jeong, S.-J. Kim, X. Zhang, T. Shim, and J.-H. Yoon, 2014: Weakening of the stratospheric polar vortex by Arctic sea-ice loss. *Nat. Commun.*, **5**, 4646, <https://doi.org/10.1038/ncomms5646>.
- Knutson, T., 2003: FMS slab ocean model technical documentation. GFDL, <https://www.gfdl.noaa.gov/fms-slab-ocean-model-technical-documentation/>.
- Lee, H. J., M. O. Kwon, S. Yeh, Y. Kwon, W. Park, J. Park, Y. H. Kim, and M. A. Alexander, 2017: Impact of poleward moisture transport from the North Pacific on the acceleration of sea ice loss in the Arctic since 2002. *J. Climate*, **30**, 6757–6769, <https://doi.org/10.1175/JCLI-D-16-0461.1>.
- Li, D., R. Zhang, and T. Knutson, 2017: On the discrepancy between observed and CMIP5 multi-model simulated Barents Sea winter sea ice decline. *Nat. Commun.*, **8**, 14991, <https://doi.org/10.1038/ncomms14991>.
- , —, and —, 2018: Comparison of mechanisms for low-frequency variability of summer Arctic sea ice in three coupled

- models. *J. Climate*, **31**, 1205–1226, <https://doi.org/10.1175/JCLI-D-16-0617.1>.
- Mahajan, S., R. Zhang, and T. L. Delworth, 2011: Impact of the Atlantic meridional overturning circulation (AMOC) on Arctic surface air temperature and sea-ice variability. *J. Climate*, **24**, 6573–6581, <https://doi.org/10.1175/2011JCLI4002.1>.
- McCusker, K. E., J. C. Fyfe, and M. Sigmond, 2016: Twenty-five winters of unexpected Eurasian cooling unlikely due to Arctic sea ice loss. *Nat. Geosci.*, **9**, 838–842, <https://doi.org/10.1038/ngeo2820>.
- , P. J. Kushner, J. C. Fyfe, M. Sigmond, V. V. Kharin, and C. M. Bitz, 2017: Remarkable separability of circulation response to Arctic sea ice loss and greenhouse gas forcing. *Geophys. Res. Lett.*, **44**, 7955–7964, <https://doi.org/10.1002/2017GL074327>.
- Mori, M., M. Watanabe, H. Shiogama, J. Inoue, and M. Kimoto, 2014: Robust Arctic sea-ice influence on the frequent Eurasian cold winters in past decades. *Nat. Geosci.*, **7**, 869–873, <https://doi.org/10.1038/ngeo2277>.
- Oudar, T., E. Sanchez-Gomez, F. Chauvin, J. Cattiaux, L. Terray, and C. Cassou, 2017: Respective roles of direct GHG radiative forcing and induced Arctic sea ice loss on the Northern Hemisphere atmospheric circulation. *Climate Dyn.*, **49**, 3693–3713, <https://doi.org/10.1007/s00382-017-3541-0>.
- Park, H.-S., S. Lee, S.-W. Son, S. B. Feldstein, and Y. Kosaka, 2015: The impact of poleward moisture and sensible heat flux on Arctic winter sea ice variability. *J. Climate*, **28**, 5030–5040, <https://doi.org/10.1175/JCLI-D-15-0074.1>.
- Peings, Y., and G. Magnusdottir, 2014: Response of the wintertime Northern Hemisphere atmospheric circulation to current and projected Arctic sea ice decline: A numerical study with CAM5. *J. Climate*, **27**, 244–264, <https://doi.org/10.1175/JCLI-D-13-00272.1>.
- Perlwitz, J., M. Hoerling, and R. M. Dole, 2015: Arctic tropospheric warming: Causes and linkages to lower latitudes. *J. Climate*, **28**, 2154–2167, <https://doi.org/10.1175/JCLI-D-14-00095.1>.
- Riahi, K., and Coauthors, 2011: RCP 8.5—A scenario of comparatively high greenhouse gas emissions. *Climatic Change*, **109**, 33–57, <https://doi.org/10.1007/s10584-011-0149-y>.
- Scinocca, J. F., M. C. Reader, D. A. Plummer, M. Sigmond, P. J. Kushner, T. G. Shepherd, and R. Ravishankara, 2009: Impact of sudden Arctic sea-ice loss on stratospheric polar ozone. *Geophys. Res. Lett.*, **36**, L24701, <https://doi.org/10.1029/2009GL041239>.
- Screen, J. A., 2014: Arctic amplification decreases temperature variance in northern mid- to high-latitudes. *Nat. Climate Change*, **4**, 577–582, <https://doi.org/10.1038/nclimate2268>.
- , and I. Simmonds, 2010: The central role of diminishing sea ice in recent Arctic temperature amplification. *Nature*, **464**, 1334–1337, <https://doi.org/10.1038/nature09051>.
- , C. Deser, I. Simmonds, and R. Tomas, 2014: Atmospheric impacts of Arctic sea-ice loss, 1979–2009: Separating forced change from atmospheric internal variability. *Climate Dyn.*, **43**, 333–344, <https://doi.org/10.1007/s00382-013-1830-9>.
- , —, and L. Sun, 2015a: Reduced risk of North American cold extremes due to continued Arctic sea ice loss. *Bull. Amer. Meteor. Soc.*, **96**, 1489–1503, <https://doi.org/10.1175/BAMS-D-14-00185.1>.
- , —, and —, 2015b: Projected changes in regional climate extremes arising from Arctic sea ice loss. *Environ. Res. Lett.*, **10**, 084006, <https://doi.org/10.1088/1748-9326/10/8/084006>.
- , and Coauthors, 2018: Consistency and discrepancy in the atmospheric response to Arctic sea-ice loss across climate models. *Nat. Geosci.*, **11**, 155–163, <https://doi.org/10.1038/s41561-018-0059-y>.
- Semmler, T., T. Jung, and S. Serrar, 2016: Fast atmospheric response to a sudden thinning of Arctic sea ice. *Climate Dyn.*, **46**, 1015–1025, <https://doi.org/10.1007/s00382-015-2629-7>.
- Sévellec, F., A. V. Fedorov, and W. Liu, 2017: Arctic sea-ice decline weakens the Atlantic meridional overturning circulation. *Nat. Climate Change*, **7**, 604–610, <https://doi.org/10.1038/nclimate3353>.
- Smith, D. M., N. J. Dunstone, A. A. Scaife, E. K. Fiedler, D. Copey, and S. C. Hardiman, 2017: Atmospheric response to Arctic and Antarctic sea ice: The importance of ocean–atmosphere coupling and the background state. *J. Climate*, **30**, 4547–4565, <https://doi.org/10.1175/JCLI-D-16-0564.1>.
- , and Coauthors, 2018: The Polar Amplification Model Intercomparison Project (PAMIP) contribution to CMIP6: Investigating the causes and consequences of polar amplification. *Geosci. Model Dev. Discuss.*, <https://doi.org/10.5194/gmd-2018-82>.
- Stroeve, J. C., V. Kattsov, A. P. Barrett, M. Serreze, T. Pavlova, M. Holland, and W. N. Meier, 2012: Trends in Arctic sea ice extent from CMIP5, CMIP3 and observations. *Geophys. Res. Lett.*, **39**, L16502, <https://doi.org/10.1029/2012GL052676>.
- Sun, L., C. Deser, and R. A. Tomas, 2015: Mechanisms of stratospheric and tropospheric circulation response to projected Arctic sea ice loss. *J. Climate*, **28**, 7824–7845, <https://doi.org/10.1175/JCLI-D-15-0169.1>.
- , J. Perlwitz, and M. Hoerling, 2016: What caused the recent “warm Arctic, cold continents” trend pattern in winter temperatures? *Geophys. Res. Lett.*, **43**, 5345–5352, <https://doi.org/10.1002/2016GL069024>.
- Suo, L., Y. Gao, D. Guo, and I. Bethke, 2017: Sea-ice free Arctic contributes to the projected warming minimum in the North Atlantic. *Environ. Res. Lett.*, **12**, 074004, <https://doi.org/10.1088/1748-9326/aa6a5e>.
- Tomas, R. A., C. Deser, and L. Sun, 2016: The role of ocean heat transport in the global climate response to projected Arctic sea ice loss. *J. Climate*, **29**, 6841–6859, <https://doi.org/10.1175/JCLI-D-15-0651.1>.
- Wang, K., C. Deser, L. Sun, and R. Tomas, 2018: Fast response of the tropics to an abrupt loss of Arctic sea ice via ocean dynamics. *Geophys. Res. Lett.*, **45**, 4264–4272, <https://doi.org/10.1029/2018GL077325>.
- Wang, M., and J. E. Overland, 2012: A sea ice free summer Arctic within 30 years: An update from CMIP5 models. *Geophys. Res. Lett.*, **39**, L18501, <https://doi.org/10.1029/2012GL052868>.
- Winton, M., 2000: A reformulated three-layer sea ice model. *J. Atmos. Oceanic Technol.*, **17**, 525–531, [https://doi.org/10.1175/1520-0426\(2000\)017<0525:ARTLSI>2.0.CO;2](https://doi.org/10.1175/1520-0426(2000)017<0525:ARTLSI>2.0.CO;2).
- , 2008: Sea ice–albedo feedback and nonlinear Arctic climate change. *Arctic Sea Ice Decline: Observations, Projections, Mechanisms, and Implications*, *Geophys. Monogr.*, Vol. 180, Amer. Geophys. Union, 111–131, <https://doi.org/10.1029/180GM09>.
- Yeager, S., A. Karspeck, and G. Danabasoglu, 2015: Predicted slowdown in the rate of Atlantic sea ice loss. *Geophys. Res. Lett.*, **42**, 10 704–10 713, <https://doi.org/10.1002/2015GL065364>.
- Zhang, R., 2015: Mechanisms for low-frequency variability of summer Arctic sea ice extent. *Proc. Natl. Acad. Sci. USA*, **112**, 4570–4575, <https://doi.org/10.1073/pnas.1422296112>.
- , and T. L. Delworth, 2005: Simulated tropical response to a substantial weakening of the Atlantic thermohaline circulation. *J. Climate*, **18**, 1853–1860, <https://doi.org/10.1175/JCLI3460.1>.